Experimental Investigation of Ice Accumulation on Horizontal Axis Wind Turbines

By:

Mustafa Ahmed Elhajare.

A thesis submitted to the School of Graduate Studies

in partial fulfillment of the requirement for the degree of

Master of Mechanical Engineering

Faculty of Engineering & Applied Science

Memorial University of Newfoundland

May 2018

St. John's Newfoundland Canada

Abstract

Wind energy is the world's fastest growing source of electricity production. If this trend continues, sites that are plentiful in wind energy will be efficiently utilized. Many sites are located in cold, wet regions such as northern coastal regions of Canada. This thesis studies ice accumulation on wind turbine blade, at several positions, for three different wind speeds at -10 ˚C and LWC of 0.6 g/m^3.

NACA 63415 airfoil was studied in this thesis. The blade model was designed to be suitable to the specifications of wind turbines. The blade was positioned at 0˚, 45˚ and 90˚, and the wind speeds were 3.5 m/s, 4 m/s and 5 m/s. In addition, some tests were conducted with changes in the angle of attack, from 0˚ to 90˚ with the angular position of the blade and wind speed maintained constant. All tests were conducted in a climatic wind chamber with a fan and two spray nozzles. Two different measurements (chord and thickness) are taken at four location of the blade span. All tests adjusted at three hours.

Therefore, these parameters produced the highest accumulation of ice on the chord and the thickness of the blade and recorded the highest weight of ice. In this study, the highest accumulation of ice on the chord and the thickness of the blade was at (V = 5 m/s, θ = 45˚ and α = 45˚) where it was approximately 61 mm and 47 mm respectively, and the maximum weight of ice on the blade was 6.7 kg. When the angle of attack changed, the weight of the ice increased slightly, where the highest ice weight at the angle of attack of 90˚ was 7.2 kg.

Acknowledgement

I am deeply indebted to my thesis supervisors and research advisors; Dr. Kevin Pope, Assistant Professor of Mechanical Engineering, and Dr. Xili Duan, Assistant Professor of Mechanical Engineering. Grateful acknowledgment is due for their sincere support, valuable guidance, fruitful discussions, and comments throughout this study. I would like to thank them for giving me this great opportunity; it was a rewarding experience, both professionally and personally.

I would like to thank the staff at Mechanical Department Laboratory who have helped me a lot, made my work easier, and added pleasant moments to my work.

I wish to acknowledge the support and cooperation of my colleagues, and classmates during my study at Memorial University.

I would also like to thank my parents, my brothers, and my sisters. These people supported me throughout my studies and encouraged me when needed.

Contents

List of Figures

List of Tables

1. Chapter - Introduction

Wind energy has developed considerably during the last few years. It is used increasingly in many locations around the world, especially in cold regions [Laakso et al., 2009]. The best locations for wind farms are in cold regions with higher elevations, because for each 100 m of elevation in the initial 1000 m, there is an increase of 0.1m/s of wind speed (Lamraoui el at., 2014). The possibility of wind power in other regions is less than that in cold regions, by about 10%, for two reasons. Firstly, air density in cold regions is greater than that of warm regions. Secondly, the kinetic energy will rise, which leads to increasing wind power production (Lamraoui el at., 2014).

Locations with a high elevation, such as mountains and coastal areas are exposed to ice in the cold seasons, although these locations are usually favourite sites for wind turbine farms (Lamraoui el at., 2014). Arctic and sub-arctic areas present significant issue's, such as atmospheric icing. These areas are also exposed to atmospheric ice as are in high regions (Haaland, 2011). Increasing the performance of wind turbines in icing conditions is necessary to improve the profitability of wind power plants. Ice growth with variations in the atmospheric temperature and water droplet sizes are important factors, as they affect energy production (Homola, et al., 2010).

Problems on wind turbines occur due to ice accretion, including the reduction of power due to the disrupted aerodynamics, overload due to delayed stall, and increased fatigue of components due to imbalance in the ice load (Homola, et al., 2010). A negative effect of ice accumulation on wind turbine blades is that causes distortion to the blades profile. This distortion frequently does not depend on the amount of ice accretion but on the location that accrues it; a small amount of ice accretion on the front edge of the blade

will minimize the aerodynamic properties significantly and affect the power output (Lamraoui el at., 2014).

Canada has a cold climate, where ice is one of the greatest difficulties in the operation of wind turbines. According to measurements by Natural Resource's Canada, in north Canada, ice accretion can occur up to 20% of the time, between November and April (CanWEA 2015). Additionally, in Canada the power capacity of wind is anticipated to rise from 0.4 G in 2004 to 8.5 GW in 2020, and is expected to reach about 6% of total power generation, and for overall electrical power, about 3.6%, as indicated via Natural Resource's Canada (CanWEA 2015).

1.1 Literature review

As wind energy projects in cold climate are growing and developing, the surfaces of wind turbine blades are exposed to icing. The relationship between the force of adhesion and temperature is approximately linear, increasing about 6000 kg/m^2 for each degree centigrade decrease in temperature. There are two distinct types of ice: glaze and rime, and, each has different characteristics. Usually, there will be a mixed icing regime that is a combination of these two types (Kraj and Bibeau, 2010). Reducing the uncertainty regarding wind turbine performance in icing conditions, improves the profitability of wind power installations. The ice growth changes with variations of the atmospheric temperature and water droplet size (Homola, et al., 2010). Ice accretion on a wind turbine occurs when super cooled liquid water droplets in fog and clouds collide with it. In addition, ice accretion on the wind turbine blades stops operations of the turbine because the ice changes the shape and mass of a blade. To know how ice accretion affects

a wind turbine, the amount of ice accretion on a wind turbine should be determined (Fikke, 2006).

Ice accretion on a wind turbine differs, depending on location and latitude, which effects the wind turbine fatigue loads. In addition, ice accretion might cause wind turbine vibration, which leads to other serious damage such as structure failure (Alsabagh, el al., 2013). In addition, ice accretion causes several problems on wind turbines, such as loss of power due to the disrupted aerodynamics, overload caused by delay stall, and increased fatigue of components due to imbalance in the ice load (Homola, et al., 2010). The external conditions at a cold climate site have several effects on the wind turbine behaviour and consequently, on the efficiency of a wind farm. One of these issues is a probable change of the fatigue load level (Frohboese et al., 2007).

Parent and Ilinca, (2011) indicated that ice evaluation can be conducted with multiple measurements of wind speed and relative humidity, and icing detection with ice sensors and a power curve check during operation. Standard measurement data were used to estimate the parameters needed for ice loading and ice accretion on wind turbines rotor blades, especially the ice vane length and the ice masses, which lead to results that need to be explained carefully prior to being applied to the fatigue load calculation (Frohboese et al., 2007). Also, the best method for defrosting is to use special paint with active heating elements (Parent and Ilinca, 2011). Some possible mitigation strategies, include special daubing to help to melt ice or using heat to thaw ice (Fikke, 2006). To reduce ice accretion, an ice phobic surface coating is most effective to the de-icing thermal regime. To control the ice accumulation rate, the profile shape extension has to be effectively mitigated for glaze ice with the least effort (Kraj and Bibeau, 2010).

According to Antonini el at. (2011) ice does not only affect wind turbines, it is also problematic in many areas such as aeronautics, offshore oil platforms, and power lines. Although presently available mechanisms for ice removal are mostly effective, they need a continuous supply of heat, chemicals, or electrical power. Moreover, the convenient conjunction coatings on aerodynamic and structural surfaces can either enhance the standard anti / de-icing system or lead to a substantial reduction of the energy consumption of present systems. A possible solution to prevent ice accretion is to use super hydrophobic coating to take advantage of its ability to repel water and lesson the adhesion of drops in a liquid state (Antonini el at., 2011).

The icing on wind turbine blades surfaces effects wind turbine performance and safety. These negative effects mainly include changing the load on a blade, affecting the aerodynamics forces, and reducing the torque and power output. The icing distribution has different effects on the attack angles of the blade at different wind speeds. In a study (Li. Y et al., 2014), wind tunnel tests were carried out on the NASA 7715 airfoils blade of wind turbine. The authors determined that ice occurs on the blade surface when there is enough water discharge flowing in cold air. The icing area and icing rate depend on the angle of attack and wind speed. In general, the icing quantity increases with the wind speed.

Seifert and Richert used a model for ice accretion to evaluate the results of ice on rotor blades where different forms of ice have been collected and classified (Seifert and Richert, 1998). The blades were tested in a wind tunnel for both cases, clean and blade with different ice forms, where the forms were built on the front edge of the turbine blades. The impact of ice on aerodynamics and the increased fatigue were computed and

estimated, and the reduced performance because of ice forms was evaluated (Seifert and Richert, 1998).

In 2009, Øyvind Byrkjedal used maps of wind resources and icing for the same zone to evaluate the loss of power to wind turbines because of icing conditions (Øyvind Byrkjedal, 2009). He combined the wind speed and power curve for calculating the expected power output of the turbines. In addition, an icing resource map of the same zone for in-cloud icing was used to evaluate production loss. This loss was estimated to be about 14% to 22%; it depends on the process utilized to evaluate icing periods (Øyvind Byrkjedal, 2009).

In Norway and Sweden, production loss was also estimated for different location which, using wind power because of the meteorological tools errors and ice accretion on the blades (Homola et al., 2009). The authors estimated power output using wind speed measurement and compared it with power output. Ice loads were calculated repeatedly. At the most severe icing locations, these loads caused approximately 28% production loss the winter months. This ratio is large and is assumed to be underestimated, due to the uncertainty of the calculation method (Homola et al., 2009).

To calculate the annual power production losses for a wind turbine, both the wind and ice conditions must be taken into account at the same site (Tammelin and Seifert, 2001). These losses were estimated from 17% to 30% for wind turbine performance annually, and these ratios were evaluated at locations where the turbine was exposed to ice (Barber et al., 2009, Øyvind Byrkjedal, 2009 and Homola et al., 2009). There are no special icing measurements; there are only meteorological data measurements, such as temperature, wind speed and humidity. This issue is a significant challenge (Haaland,

2011). Substantiation of ice models were performed by utilizing other methods. However, ice measurements are a major challenge and still unreliable for obtaining accurate results (Haaland, 2011).

1.2 Scopes and Objectives

In this thesis, experiments are conducted to study ice accretion on wind turbine blades provide new data on the connection between ice accumulation and its effect on power production at wind farms exposed to ice accretion conditions. This research will focus on two important aspects of ice accumulation on wind turbine blades, including (i) the quantity and (ii) shape of ice accumulation on a wind turbine blade.

Earlier studies contributed in showing the impact of icing on wind turbine blades. The vast majority of these studies have addressed ice accumulation on airfoils in wind tunnels, for iced wings of an aircraft. However, such studies have to be expanded to involve operations of wind turbines in cold climate zone to achieve more understanding on accumulation of ice on wind turbine blades.

This study will focus on the effect of position of a wind turbine blade on ice accretion, where results obtained from this experiment will show the shape and amount of ice accretion on the blade. In addition, this experiment will study precipitation ice, and it is formed by freezing rain, where liquid water content is approximately 0.6 g/m^3 and droplet size is approximately 50 μm to 100 μm.

Many experimental studies based on scaled model of wind turbine blade did not consider the effect of a whole blade with twist and different chord lengths along the blade span. To obtain realistic results, this experiment takes into account the influence of twist

angle and a whole blade, and will determine the distribution of ice accretion on the blade. It will valuable new data on the quantity and shape of ice accretion on a wind turbine blade.

2. Chapter - Ice Accumulation of Wind Turbine Blades

2.1 Atmospheric Icing

There are different types of ice accumulation that can occur on wind turbines. These types are in-cloud icing, precipitation icing and wet snow accumulation. However, some sources have defined wet snow as a part of precipitation icing (Ahti, 2005). Freezing rain and freezing drizzle are defined as liquid precipitation, which occurs when air temperatures are less than or equal to 0 C˚. Other damaging icing situations are caused by wet snow, which freezes after contact, or by persistent fog or clouds (Chaîné 1974).

2.1.1 In-cloud Icing

This occurs when super cool small drops of water hit a surface below 0 C˚ and freeze upon impact. The temperature of the droplets can be as low as −30 C˚ and they do not freeze in the air because of their size. Ice accretions have different sizes, shapes and properties. They depend on the number of droplets in the air, which is refered to the liquid water content (LWC) and their size (median volume diameter — MVD). Moreover, they rely on the chord length of the blade and the collection efficiency. The most important factors are temperature, wind speed and the duration of ice formation (Fikke et al., 2006).

Glaze Ice

Glaze normally has a smooth form and transparent colour, and is formed by in-cloud icing. In addition, it is usually equally distributed on the body or surface. Glaze has a strong adhesion and a high density of about 900 kg/m^3 (ISO, 2001). This is not an effect if the surface does not freeze; however, it might run back on the surface and freeze later (Fikke et al., 2006).

Rime Ice

Rime ice is the most common type of in-cloud icing, and is created during the deposition of cloud or fog droplets, which are super-cooled (Rindeskär, 2010). Soft rime is thin ice. It accretes when the temperature is below 0 C° and the droplet size is small, which means the median volume diameter and liquid water content are small. The resulting accretion will have low density and little adhesion. Hard rime has a higher LWC and MVD, so will cause accretion with higher density, which is more difficult to remove (Fikke et al., 2006).

2.1.2 Precipitation

Precipitation icing is formed by freezing rain, freezing drizzle or snow. It usually causes much more ice accretion than in-cloud icing, and generally the results are more damaging (Homola et al., 2006). This phenomenon occurs when rain falls on a surface with a temperature below 0 C°, and often occurs during inversion. Ice density and adhesion is extensive when this phenomenon occurs (Fikke et al., 2006).

Wet Snow

Wet snow is an accumulation of snow droplets containing liquid water, and these droplets have the ability to adhere to a surface. This phenomenon occurs at temperatures above freezing. The wet snow will freeze if the temperature decreases. In this case, the physical properties such as density and adhesive strength will change. In addition, there are other influencing factors, such as wind speed and the fraction of liquid water in the snow (ISO, 2001).

Frost

Frost is formed when a water steam solidifies directly on a cool surface, and this often happens during low winds. Frost has strong adhesion and low density (Fikke et al., 2006) (ISO, 2001). Table 2.1 below shows the specifications of atmospheric icing.

Table 2:1: Typical properties of atmospheric icing (ISO, 2001).

Type of ice	Density kg/m^3	Adhesion and Cohesion	General Appearance	
			Colour	Shape
Glaze	900	Strong	transparent	equally distributed / icicles
Wet snow	300 - 600	Weak (forming) Strong (frozen)	white	equally distributed / whimsical
Hard rime	600 - 900	Strong	opaque	whimsical, pointing windward
Soft rime	200 - 600	Low to medium	white	whimsical, pointing windward

The humidity, temperature and duration of the event are the most important factors in the intervention of ice accretion. These factors are shown in Table 2.2 along with their effects on ice accretion.

Table 2:2: Meteorological parameters controlling atmospheric ice accretion (ISO,2001).

Type of ice.	Temperature of air C˚	Wind speed m/s	Droplet size	Water content in air	Typical time
Precipitation icing					
Glaze (Freezing rain or drizzle)	-10 – 0	any	large	medium	hours
Wet snow	0 – +3	any	flakes	very high	hours
In-cloud icing					
Glaze	-5 – 0	See Fig. 3.2	medium	high	hours
Hard rime	-10 – -5	See Fig. 3.2	medium	medium	days
Soft rime	-15 – -10	See Fig. 3.2	small	low	days

2.2 Modelling Ice Accretion

This research is focused on two models of ice accumulation. The first one includes several research works on ice accretion and its relationship with wind turbines. The second model provides a more accurate relationship between the cylinder and ice accretion.

2.2.1 Ice Accretion Model 1

This calculation of ice accretion is based on the collection of liquid water that freezes upon contact with a cylindrical object (Messinger, 1953). Eq. (2.1) represents the collected water mass rate of liquid water per unit surface on a cylinder.

$$M^{\cdot} = E \cdot LWC \cdot V \tag{2.1}$$

Where $M^{\cdot}$ is the collected water mass rate per unit of the surface (g/m^2.s), E is collection efficiency and V is wind speed (m/s).

According to (Walton and Woolcock, 1960), the collection efficiency can be calculated with Eq. (2.2):

$$E = \frac{St^2}{(St + 0.7)^2} \tag{2.2}$$

where St is a Stocks number and is represented by Eq. (2.3):

$$St = \frac{V.MVD^2.\rho_w}{9.\mu_a.dc} \tag{2.3}$$

MVD represents the cloud droplet medium volume diameter (μm), ρ_w is the water density (kg/m^3), μ_a is the dynamic viscosity of air (P$_a$.s) and dc is the cylinder diameter (m) that

is shown in Figure. 2.1. The ratio for dc/c is 0.024 for the NACA 63-415 airfoil (Brodkey and Hershey, 1988).

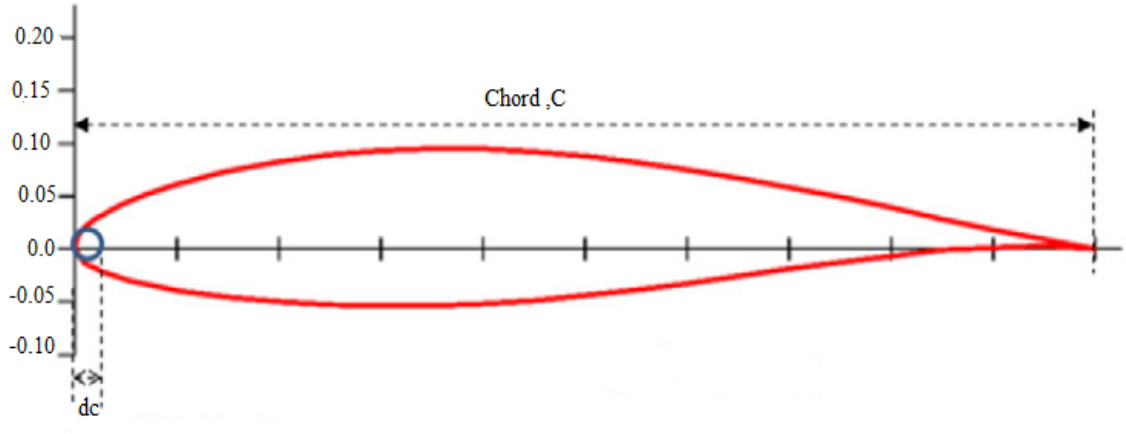

Figure 2:1: NACA 63415 (NASA, 2016).

According to (Laforte and Allarie, 1992), the ice thickness rate can be calculated using Eq. (2.4).

$$I_k = \frac{E \cdot LWC \cdot V \cdot F}{\rho_{ice}} \tag{2.4}$$

where I_k(m/s) represents the ice thickness rate, ρ_{ice} (kg/m^3) is the ice density, which is important for quantifying ice thickness. It is calculated using Laforte's ice density (Laforte and Allaire, 1992). F represents the freezing fraction of rime ice; all the supercooled water collected freezes on impact; but for glaze ice, only a fraction of super cooled water freezes on impact (Mazin et al., 2001).

2.2.2 Ice Accretion Model 2

Ice accumulation formed by frosting is usually insignificant if it is compared to ice accumulation formed by rime or glaze (Makkonen, 2000). The maximum growth rate of ice accretion (I) can be estimated using the following equation (ISO, 2001):

$$I = \frac{dM}{dt} = \eta_1 \cdot \eta_2 \cdot \eta_3 \cdot \mathrm{A} \cdot \mathrm{LWC} \cdot V_w \qquad (2.5)$$

where η_1 is the collision efficiency, η_2 is the adhesion efficiency, η_3 is the accretion efficiency, A is the cross section area of the airfoil (m^2), LWC is the liquid water content (kg/m^3), and V_w is the wind speed (m/s).

To obtain the maximum ice accretion, the three efficiencies have to be equal to unity. However, because of atmospheric conditions, the values of these efficiencies are often ranging from 0 to 1 (ISO, 2001). In addition, to obtain the successful model of ice accretion, accurate measurements and good estimations for all parameters in the Eq.(2.5) are needed. Measuring wind speed and calculating the cross section area of the airfoil are straightforward. However, the calculation of the LWC is very complex. Previous studies have shown the significance of the LWC in atmospheric icing. Therefore, calculating the amount of LWC is considered extremely important in order to measure the ice accretion rate. However, since the LWC is evaluated based on (Ronsten et al., 2009), the calculated ice accretion rate might not be accurate.

Collision efficiency

Water droplets have drag and inertial forces. These forces determine the route of droplets when these droplets move toward a cylindrical body in the air stream. These forces rely on droplet size, air stream speed and dimensions of the cylindrical body. The

drag force for small droplets will govern them because the inertia for small droplets will be weak. Therefore, small droplets will move to follow the air stream around the body. The big droplets have a strong inertial force and hence they will resist the trajectory changes (Makkonen, 2000). See Figure 2.2.

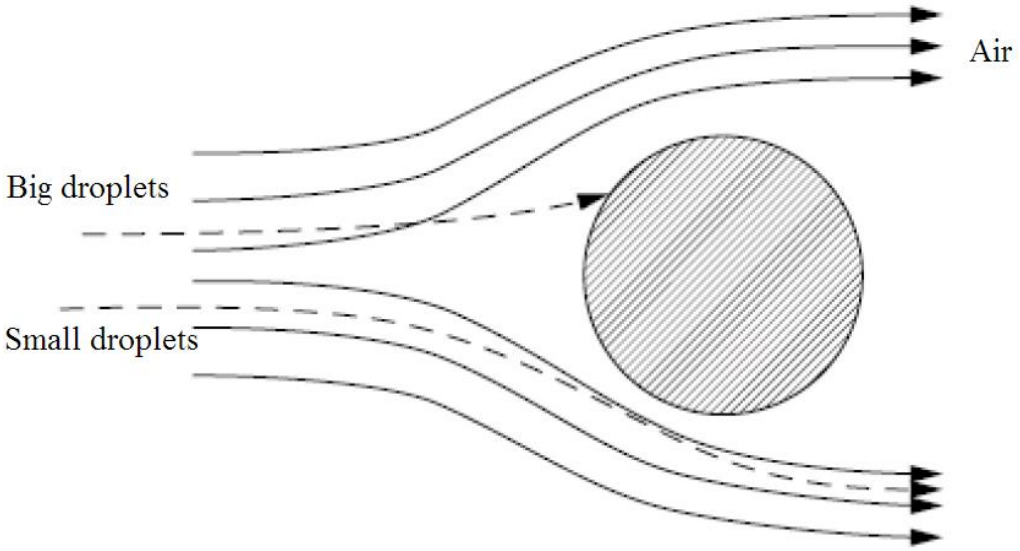

Figure 2:2: Air streamlines and droplet trajectories around a cylindrical body (Makkonen, 2000).

Langmuir and Blodgett (1946) evaluated collision efficiency for a specified size of droplets, air stream speed and cylindrical body dimensions. However, this method is inefficient because it requires many complex computational processes. However, Finstad et al (1998) simplified this method by using two dimensionless parameters to determine collision efficiency:

$$C = \frac{\rho_w \, d^2}{9\mu D} \tag{2.6}$$

and

$$\emptyset = \frac{Re^2}{C} \tag{2.7}$$

where ρ_w is the water density, d is the droplet diameter, μ is the absolute viscosity of air, D is the cylinder diameter and Re is the droplet Reynolds number, which is given by:

$$Re = \frac{\rho_a dv}{\mu} \tag{2.8}$$

where, ρ_a is the air density and v is the velocity of the free stream. The calculation of collision efficiency based on (Finstad et al., 1988) is:

$$\eta_1 = \alpha - 0.028 - \beta(\gamma - 0.0454) \tag{2.9}$$

where

$$\alpha = 1.066C^{-0.00616} \exp(-1.103C^{-0.688}) \tag{2.10a}$$

$$\beta = 3.641C^{-0.498} \exp(-1.497C^{-0.694}) \tag{2.10b}$$

$$\gamma = 0.00637(\phi - 100)^{0.381} \tag{2.10c}$$

Also, the MVD can be used to find the accurate collision efficiency when substituting the droplet diameter in equations (2.6) and (2.8). As the collision efficiency depends totally on the MVD, it can consider the collision efficiency equal to unity, such as freezing rain or wet snow, except if the body is extremely large (Finstad et al., 1988B).

Adhesion efficiency

The adhesion efficiency is represented by the ratio between the total droplets' number to the number of droplets that stick to the body. This efficiency relies on the effect of the droplets' speed, LWC and temperature (Dobesch et al., 2005). The super-cooled water droplet affects efficiency of adhesion in terms of dry and wet growth. Dry

growth represents water droplets hitting an iced surface, and wet growth represents water droplets hitting an iced surface with a liquid layer.

The adhesion efficiency can be calculated with the following equation:

$$\eta_2 = \frac{1}{v} \tag{2.11}$$

where v is the wind speed (m/s). $\eta_2 \approx 1$ when v is less than 1 (m/s) (Makkonen, 2000). When the snowflake's surface is wet, η_2 is bigger than zero for snow particles alone. Therefore, this phenomenon is useful for determining the period of wet snow events since there is no ice accretion (η_2=0) (Makkonen, 2000).

Accretion efficiency

The accretion efficiency will be equal to unity when the ice is dry (rime ice). In the glaze ice case, the accretion efficiency will depend on the latent heat rate, which is transferred from the surface's body to the air during the liquid water phase (Makkonen, 2000).

According to previous studies, the accretion efficiency can be estimated if the heat balance of the surface is considered, and it can be calculated by this equation:

$$Q_f + Q_v = Q_c + Q_e + Q_l + Q_s \tag{2.12}$$

where Q_f is the latent heat emitted during freezing, Q_v is the frictional heat of air, Q_c is the heat loss due to the air, Q_e is the heat loss because of evaporation, Q_l is the heat loss in the warm water due to the freezing temperature, Q_s is the heat loss due to radiation (Makkonen, 2000).

The latent heat emitted affects wet growth and dry growth, and is represented as:

$$Q_f = IL_f \tag{2.13a}$$

$$Q_f = (1 - \lambda)\eta_3 F L_f \qquad (2.13b)$$

where I represents the density of icing, L_f is the latent heat of fusion, λ represents the liquid fraction of the accretion, and F is the flow density of water to the surface, where it can be calculated by the following equation:

$$F = \eta_1 \eta_2 LWCV_w \qquad (2.14)$$

Previous studies have shown that the liquid fraction (λ = 0.26) is logical as the first assumption because it is not sensitive to the growth conditions (ISO, 2001) (Makkonen, 2000).

The frictional heat of air is usually small; therefore, it is often neglected. However, it is represented as the following equation:

$$Q_v = \frac{hrV_w^2}{2C_p} \qquad (2.15)$$

where r is the extraction coefficient for viscous heating, and is equal to 0.79 for a cylinder based on (ISO, 2001), V_w is the wind speed, C_p is the specific heat capacity of air and h is the convective heat transfer coefficient (Makkonen, 2000). This coefficient is often estimated using cylindrical body models; therefore, it is generally a good estimation for icing bodies.

The convective heat transfer is shown as:

$$Q_c = h(T_s - T_a) \qquad (2.16)$$

where T_a is the temperature for the surrounding air and T_s is the temperature of body's surface that is zero for wet growth (ISO, 2001).

The evaporation heat transfer can be parameterized as:

$$Q_e = \frac{h\varepsilon L_e(e_s - e_a)}{C_p P} \qquad (2.17)$$

where ε is the molecular masses' ratio of dry air to water vapour, and is equal 0.622. L_e is the latent heat of vaporization. e_s is the saturation water vapour pressure over the accretion surface for in this situation, e_s is a constant and its value is 0.617 kPa, e_a is the function of temperature and relative humidity, and is usually assumed to be 100% in clouds (Makkonen, 2000).

The heat loss in the warm water to the freezing temperature can be calculated with this equation:

$$Q_l = Fc_w(T_s - T_d) \tag{2.18}$$

where c_w represents the specific heat capacity, and T_d is the droplets' temperature. It could be assumed that T_d equals T_a if these droplets come from a cloud. However, this assumption is also used for super cooled droplets.

The heat loss due to radiation is given by:

$$Q_s = a\sigma(T_s - T_a) \tag{2.19}$$

where a is the radiation linearization constant, and σ is the Stefan-Boltzmann constant. They are 8.1×10^{7} and 5.67×10^{-8} ($W.m^{-2}.k^{-4}$) respectively.

This equation only considers long-wave radiation because short-wave radiation often occurs in cloudy weather. Therefore, it can be neglected. In addition, in this case, it can be assumed that the ice surface and environment are black body radiation.

Combining equation (2.13b) and (2.18) into equation (2.12) and solving the accretion efficiency, η_3,result in:

$$\eta_3 = \frac{1}{F(1-\lambda)L_f}\left[(h+6a)(T_s - T_a) + \frac{h\varepsilon L_e}{C_p p}(e_s - e_a) - \frac{hrV_w^2}{2C_p} + FC_w(T_s - T_d)\right] \tag{2.20}$$

In conclusion, the rate of ice accretion (I) can be calculated with the Eq. (2.9), Eq. (2.11) and Eq. (2.20). Additionally, the wind speed, LWC, and the area of the body are known.

2.3 Effect of Icing on Blade Profiles

Ice accretion on the wind turbine's blade profiles has a range of shapes resulting from different temperature and heat balance situations (Gent et al., 2000).

The effect of ice accretion on the blade profile is generally an altered profile shape, resulting in a reduced lift coefficient (C_l) and increased drag coefficient (C_d) (Holdo et al., 1997).

The result of these changes for a wind turbine blade profile can be seen in the in-plane (rotating) force:

$$F_y = (C_l \sin \emptyset - C_d \cos \emptyset) \frac{1}{2} \rho W^2 C(r) \tag{2.21}$$

where ρ (kg/m3) is the air density, W (m/s) the air velocity relative to a point on the rotating blade of the angle between the plane of rotation and the relative air velocity and c (m), the chord at radius (r), is reduced both from the decrease in C_l and the increase in C_d.

For analysis, a torque coefficient:

$$C_y = C_l \sin \emptyset - C_d \sin \emptyset \tag{2.22}$$

was defined, and the changes in the aerodynamic forces acting on the blade profile are illustrated in Figure. 2.3.

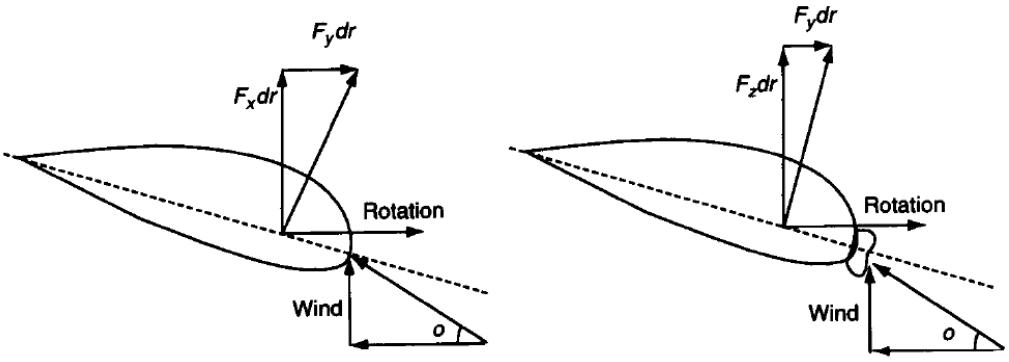

Figure 2:3: Wind turbine profiles with and without ice, illustrating the reduced torque in the case of leading edge accretion.

2.4 Damage from Icing on Wind Turbine

Ice accretion causes many issues for a wind turbine. The following problems are directly related with the wind turbines:

2.4.1 Electrical and Mechanical failure

The ice accretions on the nacelle lead to condensation in the electronics at a higher temperature. The ice accretion causes much mechanical damage, such as imbalance between blades, high vibrations and overload on the blades and tower structure. Operation at low temperatures affects oil viscosity and changes the dimensions and mechanical properties of different components of the wind turbines. This results in possible overheating and higher fatigue charges on components; one of the most affected being gearboxes, which lifetime is considerably reduced (Botta et al., 2005).

2.4.2 Measurement errors

In the assessment stage, ice accretion affects measurement tools such as the anemometers, temperature sensors and wind vanes. In icing conditions, wind speed

errors can be as high as 30% (Laakso et al., 2003). Another study identifies a maximum error of 40% for an ice-free anemometer and 60% for a standard anemometer during icing events (Fortin et al., 2005).

2.4.3 Power losses

Ice accretion changes the shape and roughness of the blade airfoil, consequently affecting aerodynamic characteristics and introduces measurement errors from turbine instruments, such as a wrong wind speed or direction, which affects the yaw and power controls. Small amounts of ice on the leading edge of airfoils significantly reduces the aerodynamic properties of the blade and the resulting power production (Marjaniemi and Peltola, 1998). Power losses may up to 50% of the annual production, depending on icing intensity and its duration on the site, the type of wind turbine model and the evaluation methodology (Tammelin et al., 2005).

3. Chapter - Wind Turbine Performance Indicator

3.1 Wind Power

Wind power is the conversion of the kinetic energy of the wind into electrical power by wind turbine (Haaland, 2011). As is known:

$$\text{Kinetic energy} = \frac{1}{2}mV^2 \tag{3.1}$$

where *m* is mass (kg) and V *is* velocity (m/s). The mass flow rate of the air can be represented by $\mathrm{m} = \rho \mathrm{AV}$. Where ρ is the density of air (kg/m^3), A is a cross section of the area swept by the rotor (m^2) and V is wind speed (m/s). Then the power of wind can be represented by:

$$P_w = \frac{1}{2}\rho A V^3 \tag{3.2}$$

At higher sites, such as mountainous areas, air density is less than average; however, in cold climates the average density might be higher by 10% (Boyle, 2004). In addition, these, along with higher air density, lead to increasing the production up to 16% in cold regions (Jasinski et al., 1998). Typical horizontal wind turbines have three blades (Manwell et al 2010). Each wind turbine has an efficiency factor which is usually called the power coefficient, Cp,

3.2 Wind Turbines

A wind turbine is a device that converts kinetic energy from the wind into electrical power. Today, horizontal wind turbines have three blades and are being used increasingly to create power (Manwell et al 2010). Figure 3.1 shows the horizontal wind turbine with its main parts.

Based on Manwell et al., 2010, which explains an ideal turbine construction, a wind turbine consists of a tower, rotor and nacelle. The Rotor is considered the most important part of a wind turbine and includes the blades and hub. The Nacelle is a cover that protects the internal parts from weather conditions, and includes a generator, Drive Train (Transmission) and control system. The transmission group consists of three main parts, the gearbox, low-speed shaft, and high speed shaft. The low-speed shaft connects the rotor and the gearbox and the high-speed shaft between the gearbox and generator. The gearbox converts the low rotation to a higher rotation from the rotor to the generator. The generator is a device that converts the mechanical power to electrical power; most turbines use induction or a synchronous generator. The Yaw system works to direct the blades so that the turbine can utilize the wind as much as possible. The tower is what holds the nacelle and rotor. Elevation of the tower is usually two or three times the rotor's radius. Inside the tower are stairs that allow access to the nacelle for maintenance work. The foundation of the tower is solid and well installed in the ground to maintain the wind turbine's stability.

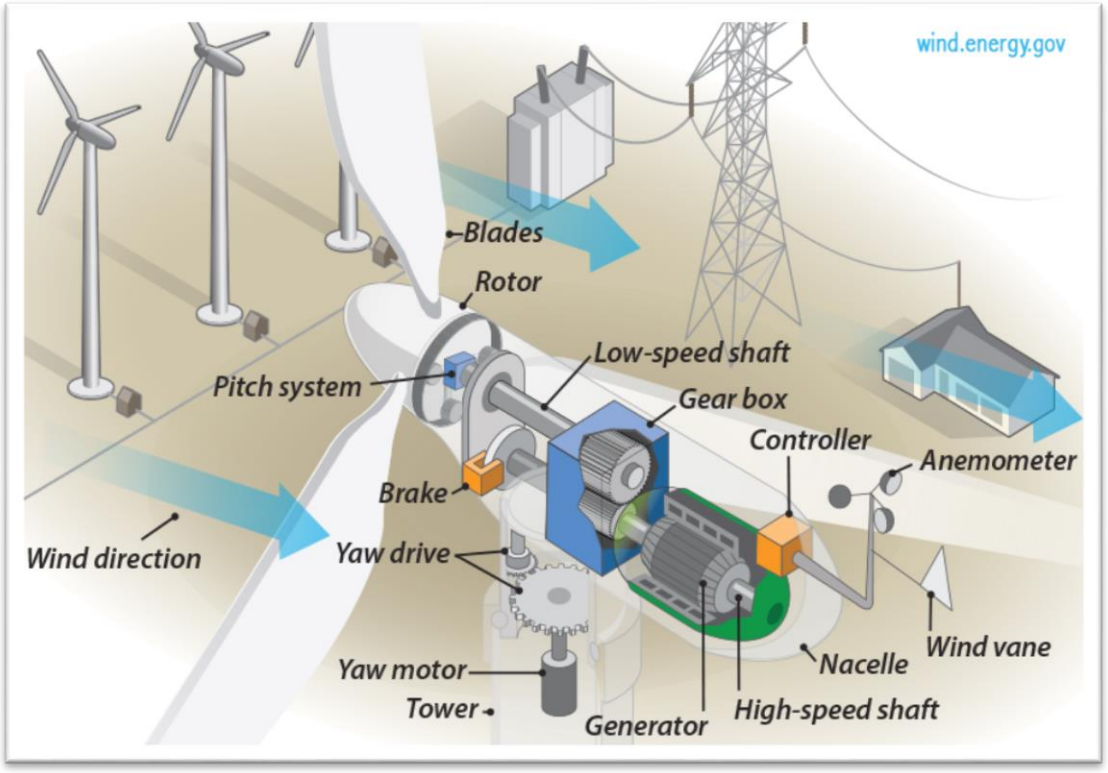

Figure 3:1: Model build-up of a Horizontal Wind Turbine (Manwell et al., 2010).

3.3 How Wind Turbines Extract Energy

The turbine's blades rotate when the wind hits them. Conversion of 100% wind power to 100% electrical power is impossible because of physical laws; the maximum energy that can be generated is about 59%. This ratio is called the Betz limit (0.59) (Manwell et al., 2010). Each wind turbine has an efficiency factor which is usually called the power coefficient, Cp, it is lower than 0.59.

$$P = P_w C_P \tag{3.3}$$

The power production by a wind turbine is measured by the equation above. Modern three-bladed wind turbines usually have a Cp rate between 0.4 and 0.5, as friction forces

in the rotor or axle shaft will decrease turbine efficiency. According to Boyle- 2004, the tip speed ratio is a function of the blade speed and the wind speed:

$$\lambda = \frac{\omega R}{V_w} \tag{3.4}$$

where λ is the tip speed ratio, ω is the velocity of rotation of the rotor, R is the radius of the rotor and V_w is the wind speed.

3.4 How to Design a Wind Turbine Blade

The angle of attack and the lift and drag coefficients are important factors to express the forces on the blades of a wind turbine (Hansen and Butterfield, 1993). The relationships of forces, speeds and angles of the blade are shown in Figure 4.1.

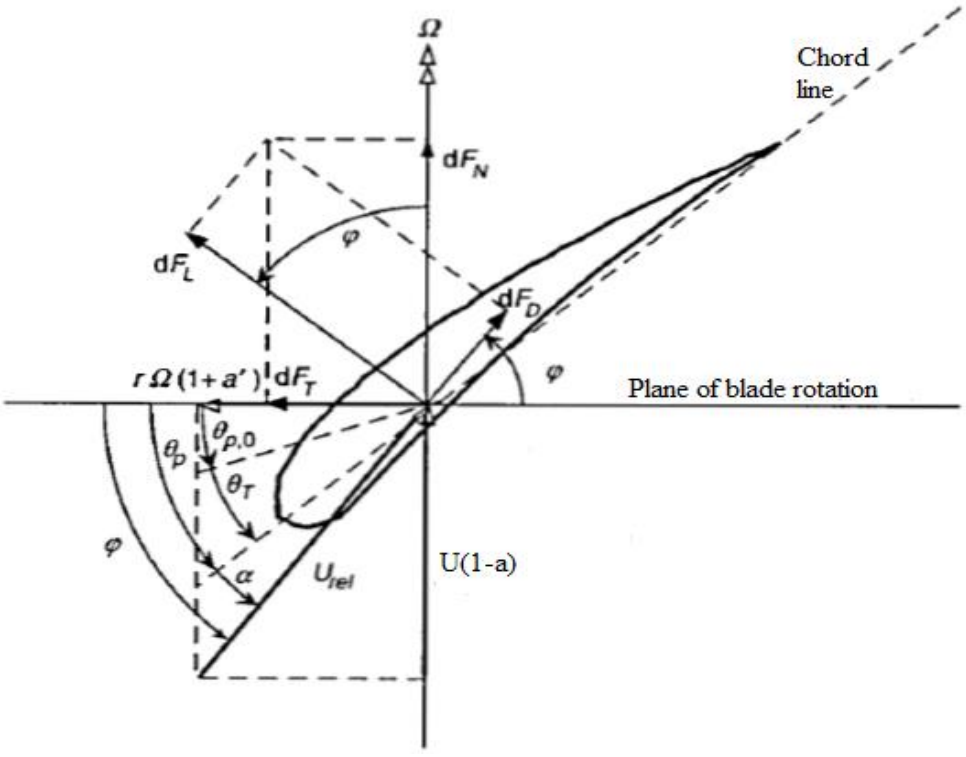

Figure 3:2: Analysis of blade geometry of horizontal axis of wind turbine (Manwell el at., 2010).

φ is the angle of relative wind; dF_L is the incremental lift force; dF_D is the incremental drag force; dF_N is the incremental normal force to the rotation plane; dF_T is the incremental tangential force to the circle swept via the rotor, which is a useful force to create useful torque. θ_P is the section pitch angle, which is its position between the chord line and the plane of rotation; θ_T is the blade twist angle; α is the angle of attack, which is the angle between the chord line and the relative wind; $\theta_{p,0}$ is the blade pitch angle at the tip (Manwell el at., 2010).

The blade shape of the wind turbine is different varies for an ideal rotor without wake rotation and for an optimum rotor with blade rotation. Each one has equations to calculate the chord and twist angle for the blade (Manwell el at., 2010). In this thesis, I designed the blade shape of wind turbine with wake rotation. The impact of wake rotation can be calculated using the analysis developed for a general rotor. In this case, assume the drag coefficient Cd and tip losses equal one unit (Manwell el at., 2010). The partial derivative of this part of the integral for the C_p equation is:

$$C_p = \left(\frac{8}{\lambda^2}\right)\int_{\lambda_h}^{\lambda} sin^2\varphi\ (\cos\varphi - \lambda_r \sin\varphi)(\sin\varphi + \lambda_r \cos\varphi)\{1 - (\frac{C_d}{C_l})\cot\varphi\}\ \lambda_r^2\, d\lambda_r \qquad (3.5)$$

Then

$$\frac{\partial}{\partial\varphi}\{sin^2\varphi\ (\cos\varphi - \lambda_r \sin\varphi)(\sin\varphi + \lambda_r \cos\varphi)\} = 0 \qquad (3.6)$$

yields:

$$\lambda_r = \sin\varphi(2\cos\varphi - 1)/\{(1 - \cos\varphi)(2\cos\varphi + 1)\} \qquad (3.7)$$

Further:

$$\varphi = \left(\frac{2}{3}\right)\tan^{-1}\left(\frac{1}{\lambda_r}\right) \tag{3.8}$$

$$C = \frac{8\pi r}{BC_l}(1 - \cos\varphi) \tag{3.9}$$

The optimum values for φ and C, including wake rotation, are represented via equations (4.21), (4.22) respectively (Manwell el at., 2010).

Solidity is the ratio of the platform area of the blades to the swept area, thus:

$$\sigma = \frac{1}{\pi R^2}\int_{r_h}^{R} C\ dr \tag{3.10}$$

If these equations are to get applied the blade shape for an optimum rotor with wake rotation, the following results, assuming λ= 5, B =3 with NACA 63-415 (airfoil data based) are obtained.

Table 3:1: Twist and chord distribution for the blade model.

r(m)	r/R	Ø (rad)	$\boldsymbol{\lambda r}$	c(m)	Ø (deg)	Section pitch	Twist angle
0.094	0.1	0.74	0.5	0.26	42.29	37.04	34.75
0.187	0.2	0.52	1	0.27	30	24.75	22.46
0.281	0.3	0.39	1.5	0.23	22.46	17.21	14.92
0.374	0.4	0.31	2	0.19	17.71	12.46	10.17
0.468	0.5	0.25	2.5	0.16	14.53	9.284	6.994
0.561	0.6	0.21	3	0.14	12.29	7.04	4.750
0.655	0.7	0.19	3.5	0.12	10.63	5.38	3.090
0.748	0.8	0.16	4	0.11	9.357	4.11	1.818
0.842	0.9	0.15	4.5	0.097	8.352	3.10	0.813
0.935	1	0.13	5	0.088	7.54	2.29	0.00

This design of blade is efficient but complex and costly to build. However, if blade form is determined to have a uniform taper, such that the tip part of the blade corresponds closely to the root. Therefore, a straight line is drawn through the 70% and 90% span points, as shown in Figure 3.3 and 3.4, which not only simplifies the blade form but also removes much of the material close to the root (Burton el at., 2011).

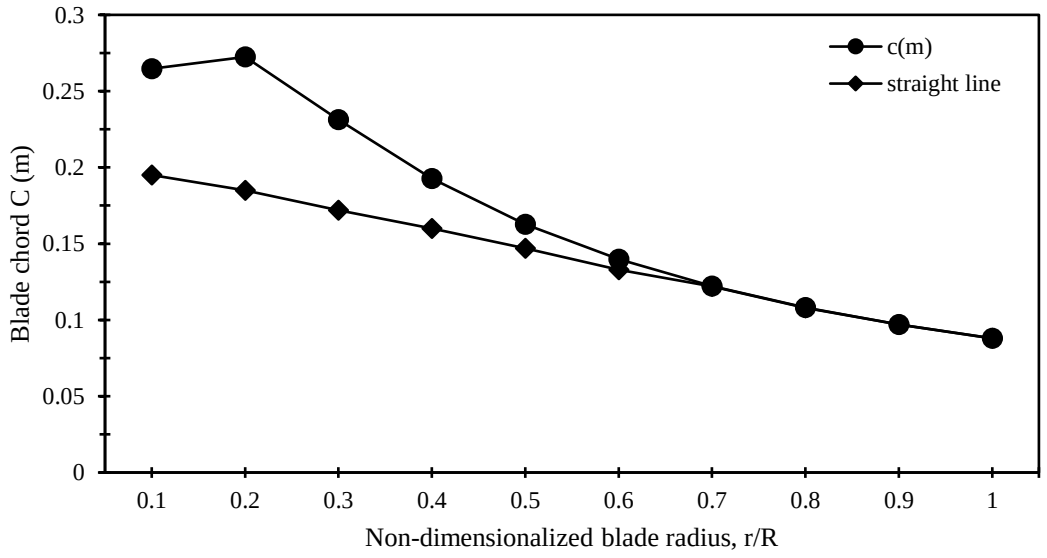

Figure 3:3: Optimum of wind turbine blade design with straight line.

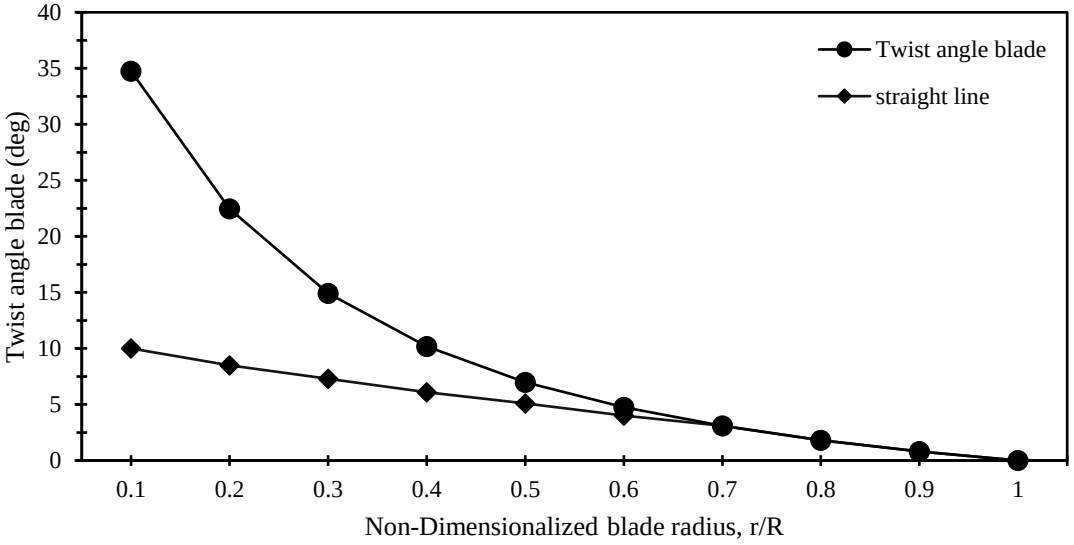

Figure 3:4: Optimum of wind turbine blade design with straight line.

4. Chapter - Experimental program

4.1 Methodology

The experiment will be accomplished in a cold chamber with dimensions of 25ft, 15ft and 15ft. In addition, a small wind turbine blade is used 19 cm max, and 8.3 cm min for the chord. The cold air is pushed into the cold room by the fan, and at the same time, water is sprayed from a nozzle and mixed with the cold wind. The test blade is positioned at the same height of the wind tunnel outlet. The wind speeds (V) are controlled at 3.5, 4 and 5 m/s. In this study, the cold room temperature was adjusted to -10 ℃ as shown in Table 4.1. A test blade with airfoil of NACA 415-63 is used in the experiment, as shown in Fig. 2.1. The blade is made by plastic fiber. Dimensions of the whole blade model are shown in Fig. 4.1. In this study, the digital Vernier scale is used to measure the thickness of ice accretion, a digital scale to measure the ice accumulation and photos show the shape of the ice.

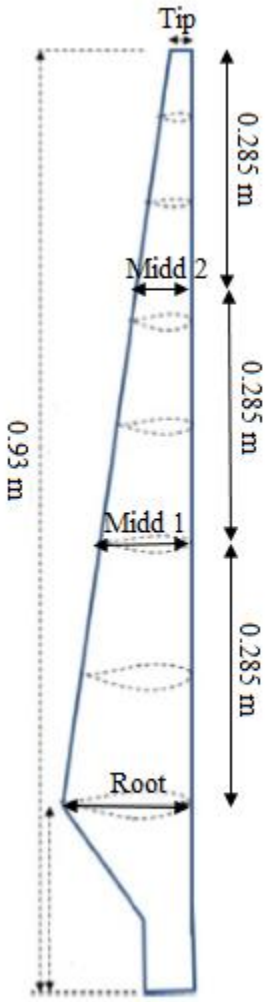

Figure 4:1: Whole blade model.

In addition, the water will be sprayed from Full Jet G and H nozzle and mixed with the cold wind. The Full Jet nozzle has a spray angle, which is standard, from 43° to 94°, narrow from 15° to 30°, and wide from 112° to 120°. In addition, it has uniform spray distribution from 0.07 to 25 gpm (0.29 to 92 lpm), and its operating pressures reach 300 psi (20 bar). See Figure. 4.2.

Figure 4:2: Full Jet G and H Nozzles.

.

The test blade is fixed at the different height from the wind fan and downstream from the outlet. In addition, the fan used in this experiment is shown in Figure 4.3.

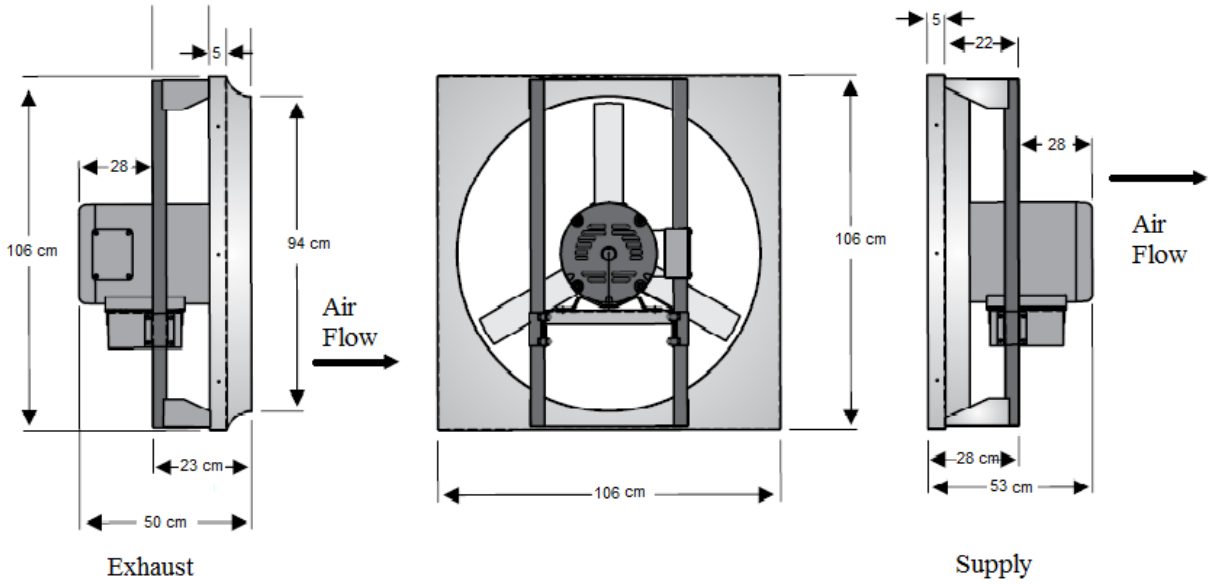

Figure 4:3: Dimensions of the Fan (S&P Canada, 2012).

4.2 Experimental setup

Experimental setup is shown in Figure. 4.4. The setup of the experiment includes the fan, spray nozzle and the blade with its stand. The positions of the blade and spray nozzle of the fan are (1.5, 0.502, 0.835) m and (0.833, 0.485, 0.321) m respectively. All coordinates are taken from the bottom left edge of the fan. Table 4.1, shows the parameters of each test. During the test, the thickness and chord of the blade are measured at four points (Tip, Mid1, Mid2, Root) six times (each 30 min) (See Figure. 4.5).

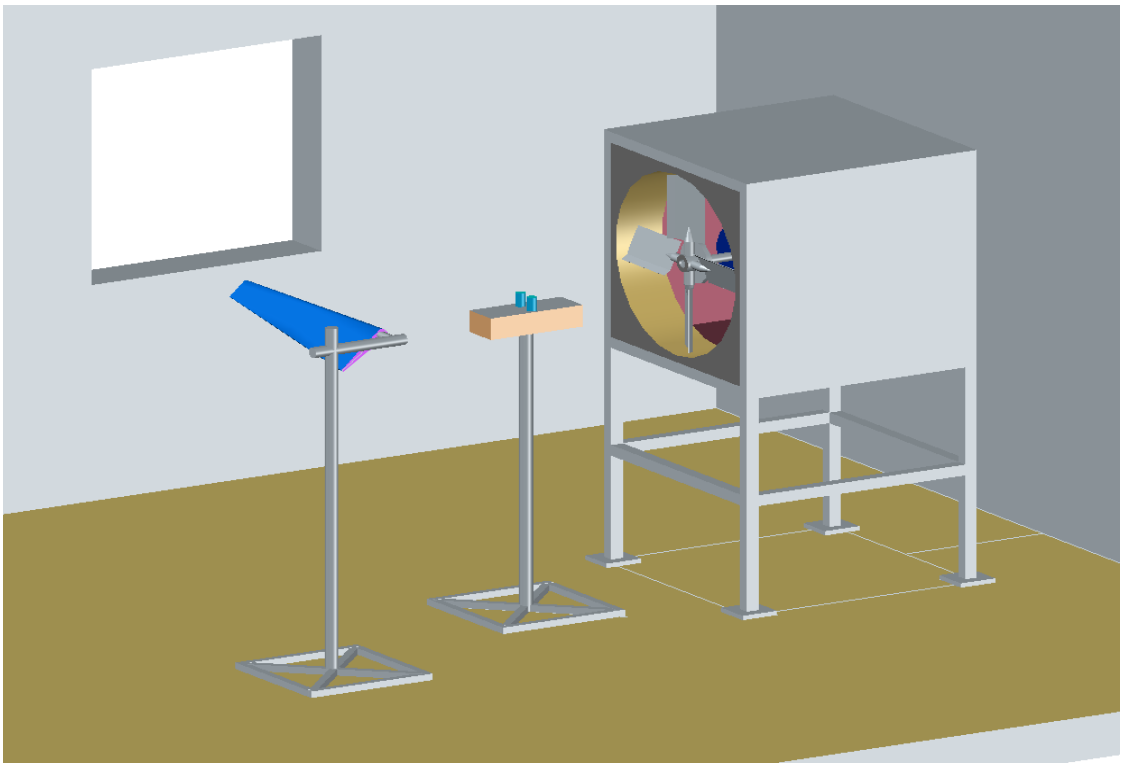

Figure 4:4: Experiment setup inside cold room.

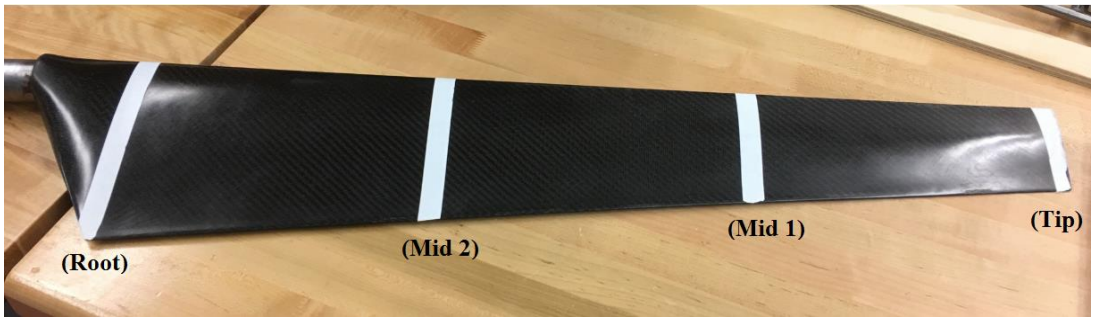

Figure 4:5: Wind turbine blade model.

Figure 4.5. depicts the wind turbine blade model. In the experiment, the spray nozzle system consists of a pump, a water tank and a timer to control the pumping of water through a tube connected to the spray. The timer controls the water volume for 5:30 seconds as the pump is pumped every five seconds, stopping every 30 seconds. The spray inside the cold chamber is shown in Figure 4.4. Note that the system is closed in the sense that the water has only one outlet, the spray.

Table 4:1: Wind tunnel simulation parameters.

Test	Temperature (˚C)	Angular Position of blade ($\boldsymbol{\theta}$)	Air velocity (V m/s)	LWC (g/m^3)	Time (hr)	droplet size (µm)	Angle of attack (α)
1	-10	0°	3.5	0.6	3	50	45°
2	-10	0°	4	0.6	3	50	45°
3	-10	0°	5	0.6	3	50	45°
4	-10	45°	3.5	0.6	3	50	45°
5	-10	45°	4	0.6	3	50	45°
6	-10	45°	5	0.6	3	50	45°
7	-10	90°	3.5	0.6	3	50	45°
8	-10	90°	4	0.6	3	50	45°
9	-10	90°	5	0.6	3	50	45°
10	-10	0°	5	0.6	3	50	0°
11	-10	0°	5	0.6	3	50	30°
12	-10	0°	5	0.6	3	50	60°
13	-10	0°	5	0.6	3	50	90°

4.3 Instrumentation of experiment

In this experiment, we used three basic equipment to measure three important parameters: ice thickness, ice weight on the blade, and wind speed measurement. This equipment are digital Vernier caliper, balance scale and wind sensor. The digital Vernier

caliper is used to measure ice accumulation on blade thickness and ice accumulation on chord of the blade. The balance scale was used to measure the weight of the snow by measuring the blade before and after the accumulation of snow. For wind speed, the wind sensor is used at four points along the blade to measure the wind at each point.

.

5. Chapter - Results and discussions

5.1 Wind Speed Tests

Prior to the start of the experiment, several tests were carried out to determine the location and proper placement of the blade. The Figures (5:1, 5:2 and 5:3) illustrate the best distribution of wind speed on the blade. The results show that the middle of the blade is exposed to maximum wind speed, which affects the ice accumulation on the blade.

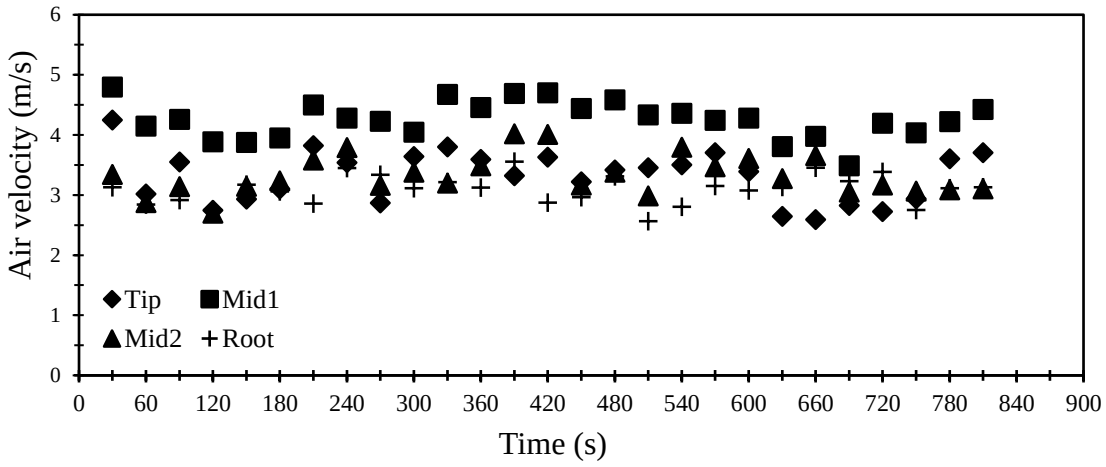

Figure 5:1: Distribution of wind speed on the blade at 45 Hz.

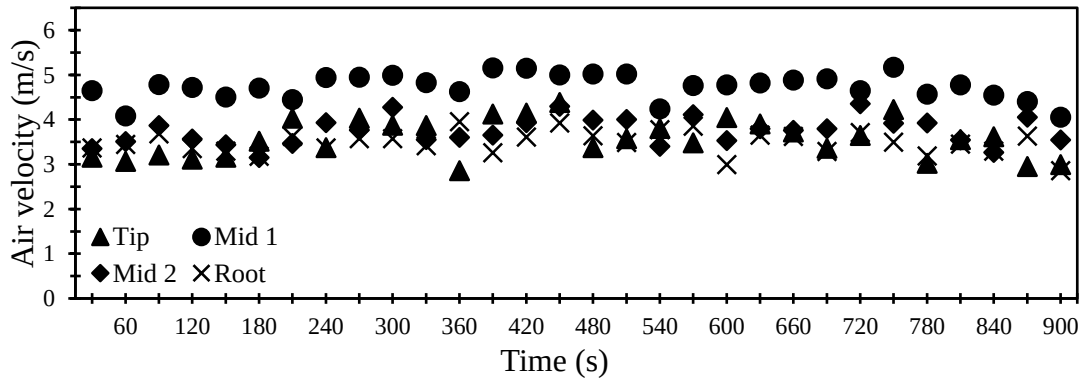

Figure 5:2: Distribution of wind speed on the blade at 50 Hz.

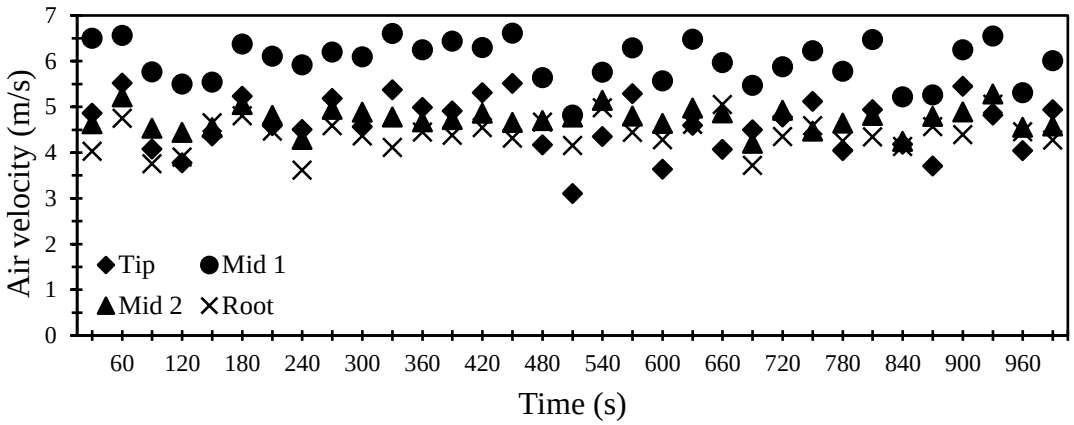

Figure 5:3: Distribution of wind speed on the blade at 60 Hz.

5.2 Blade at an Angular Position of $\theta = 0^{\circ}$ and $\alpha = 45^{\circ}$:

As shown in the results presented for Test 1 (Figure. 5:4), the greatest accumulation of ice was on the middle of blade, especially the Mid1, followed by the Mid2, while the least accumulation was at the Tip and finally at the Root. However, in (Figure. 5:5), the thickness of the ice accumulation was quite similar to that of the chord, but the accumulation of ice was lower, with a clear difference between the root and the tip of the blade. See Figure (5:6).

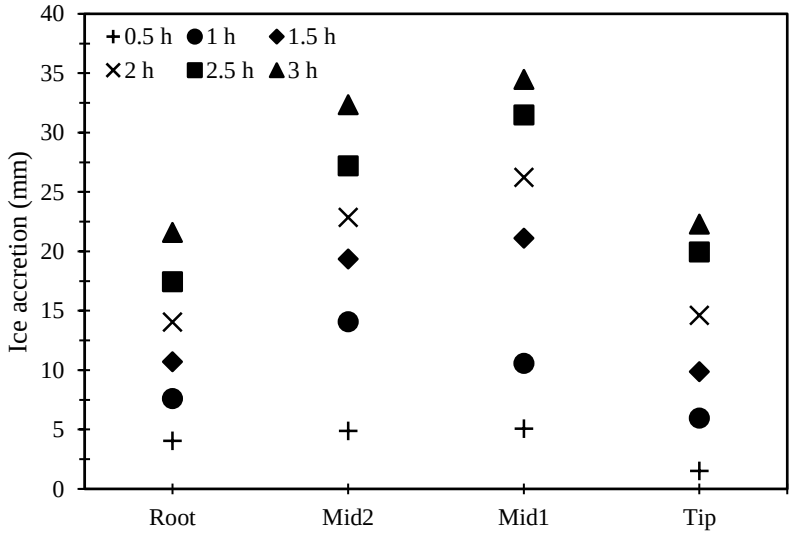

Figure 5:4: Ice accumulation for V = 3.5 m/s, θ = 0°, and α = 45˚ on the chord.

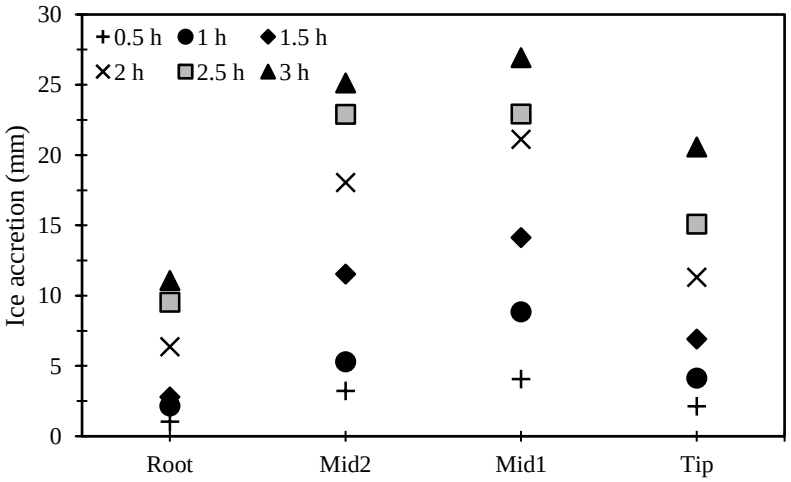

Figure 5:5: Ice accumulation for V = 3.5 m/s, θ = 0°, and α = 45˚ on the thickness.

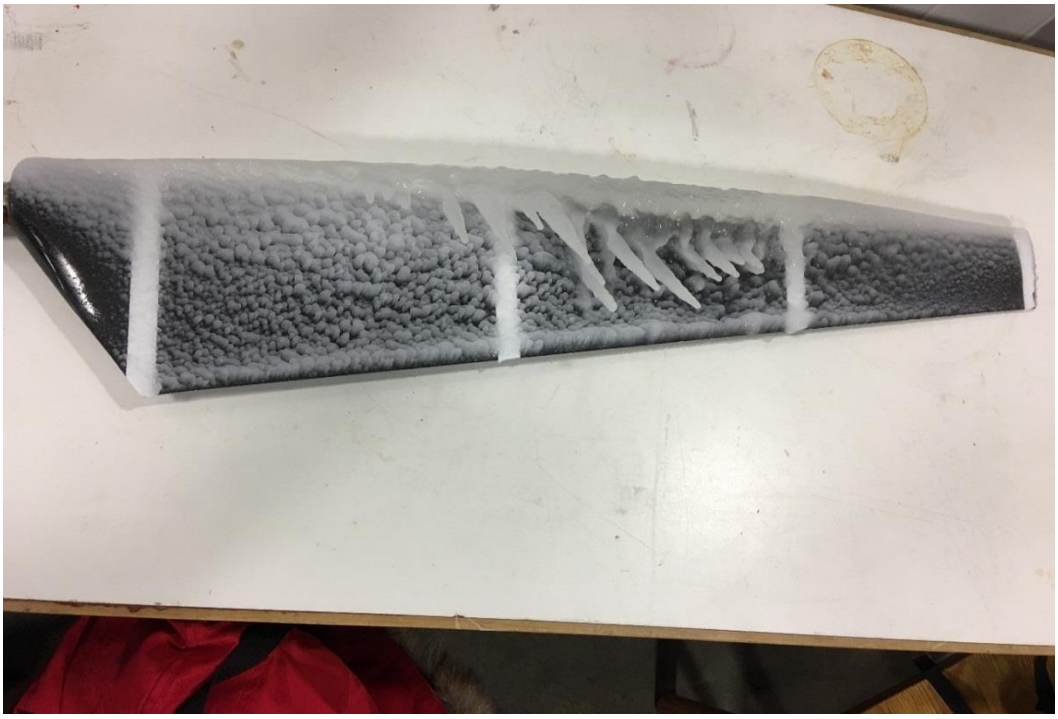

Figure 5:6: the shape of ice accumulation on the blade at V = 3.5 m/s, θ = 0°, and α = 45˚.

In this Test 2, Figure 5:7, 5:8 and 5:9 show results. These results were close at the four points of the chord. However, the difference in thickness is clear between the middle of the blade and its edges (Root and Tip). The Tip had less accumulation of ice than did the Root, contrary to what occurred in Test 1.

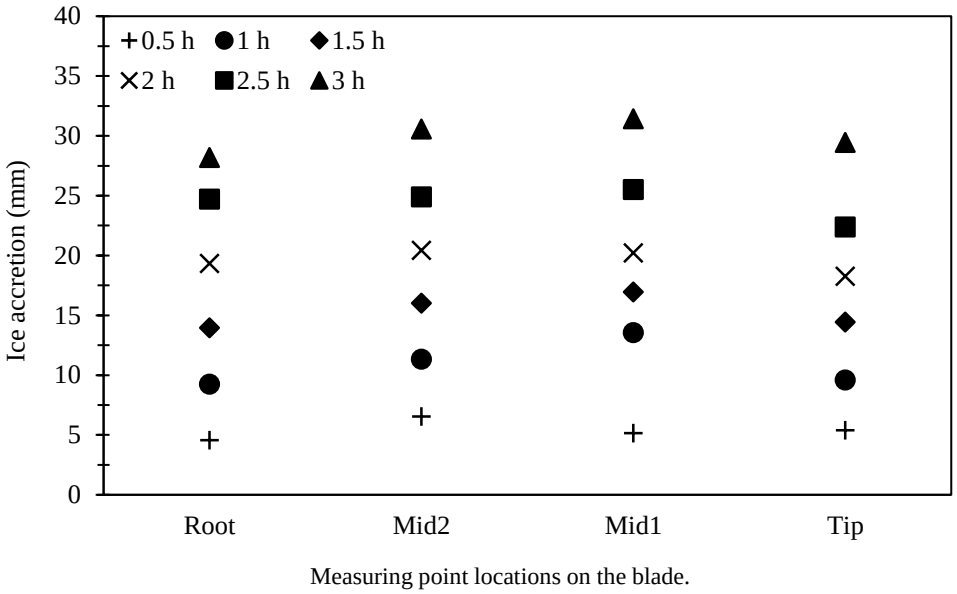

Figure 5:7: Ice accumulations for V = 4 m/s, θ = 0°, and α = 45˚ on the chord.

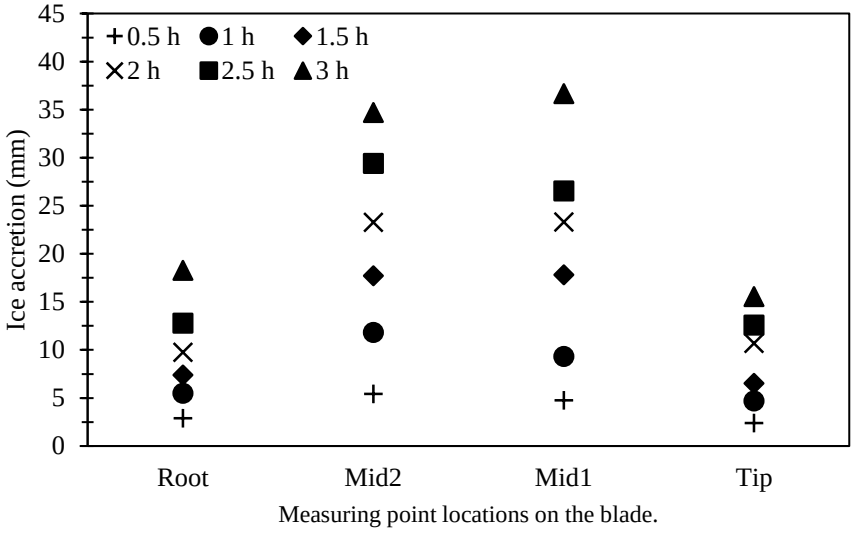

Figure 5:8: Ice accumulations for V = 4 m/s, θ = 0°, and α = 45˚ on the thickness.

Figure 5:9: Shape of ice accumulations on the blade at V = 4 m/s, θ = 0°, and α = 45˚.

Results of Test 3 were shown by Figures (5:10, 5:11 and 5:12). There was no difference between the results of Test 3 and Test 1 in both cases (thickness and chord); however, the ice accumulation in Test 3 was more than Test 1.

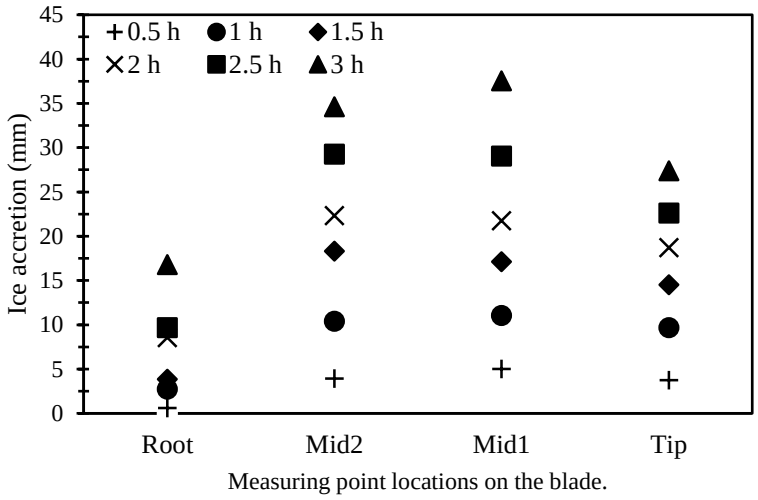

Figure 5:10: Ice accumulations for V = 5 m/s, θ = 0°, and α = 45˚ on the chord.

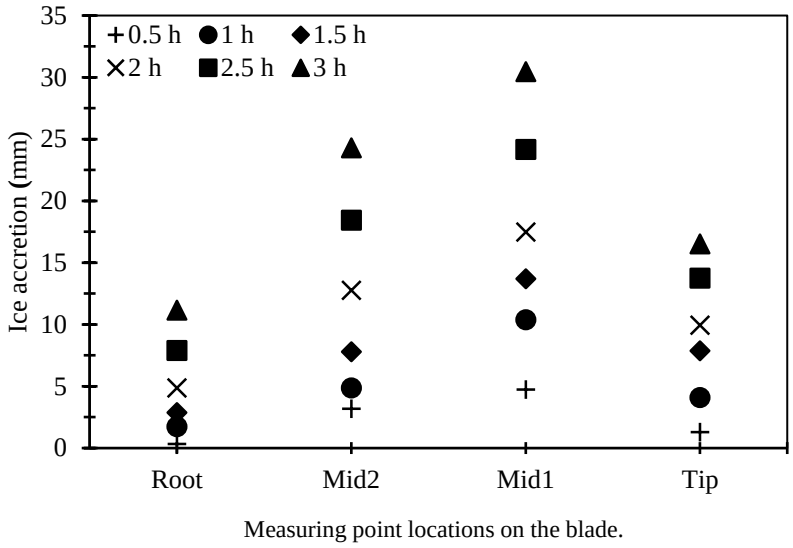

Figure 5:11: Ice accumulations for V = 5 m/s, θ = 0°, and α = 45˚ on the thickness.

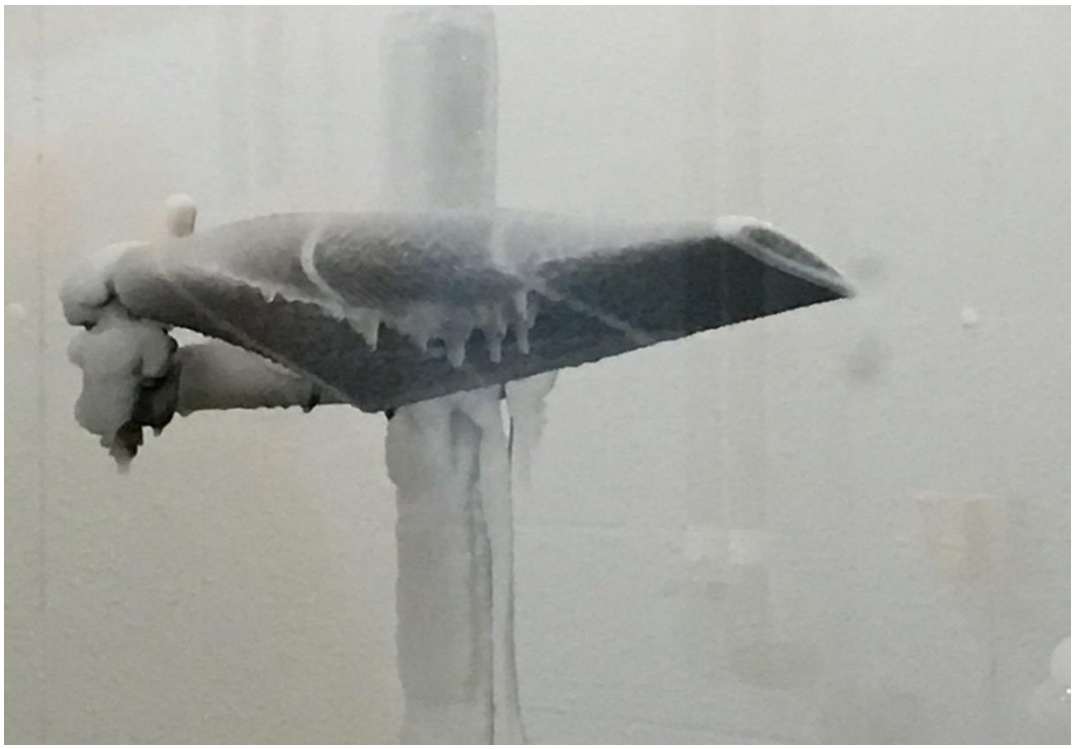

Figure 5:12: Shape of ice accumulations on the blade at V = 5 m/s, θ = 0°, and α = 45˚.

In this Figure (5:13), the ice weight on the blade is shown for each of the previous three tests (1, 2, and 3). The results showed that the largest accumulation of ice was in the third test (at 5 m/s) followed by the second test and then the first test (at 3.5 m/s), with the least accumulation of ice. These tests were at the horizontal position of the blade (0˚).

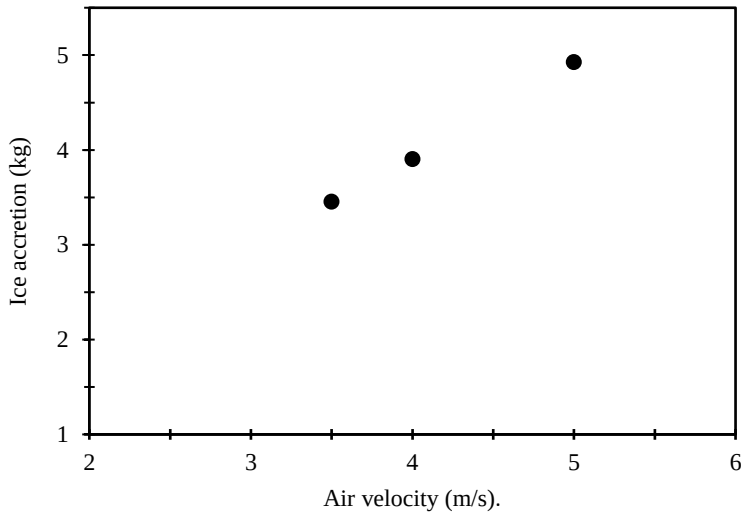

Figure 5:13: Weight of Ice accretion at θ = 0°, and α = 45˚.

5.3 Blade at an Angular Position of $\theta = 45^{\circ}$ and $\alpha = 45^{\circ}$:

This Test (4) produced different results from the previous one. Figure (5:14) shows that the greatest point of ice accumulation is Mid2, followed by the Root and then the Mid1 and finally the Tip with the least point of accumulation of ice. Figure (5:15) has the same shape as the previous arrangement with different intermediate arrangements, where the Mid1 had thicker ice accumulation than the Root, and the lowest point was at the Tip.

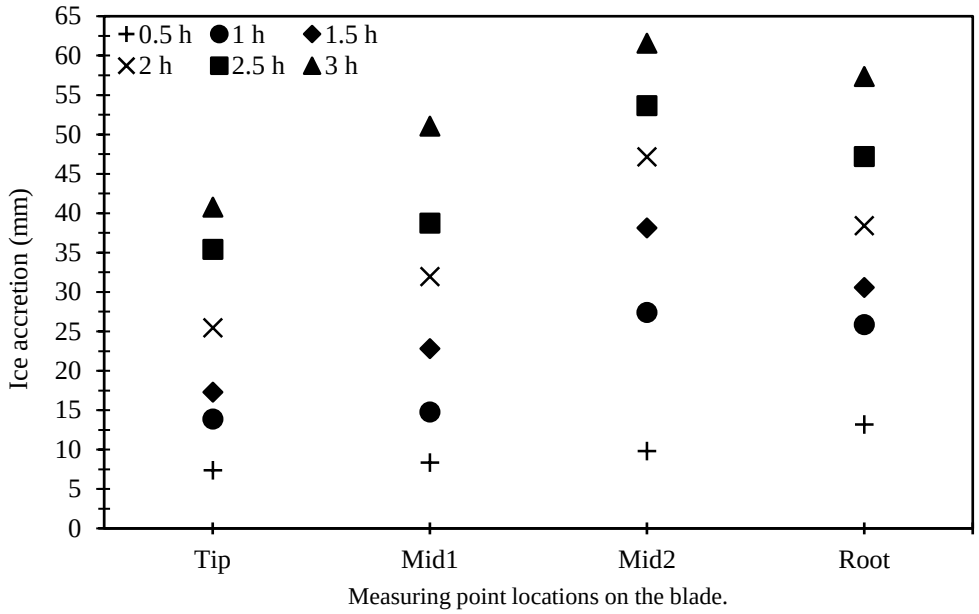

Figure 5:14: Ice accumulation for V = 3.5 m/s, θ = 45°, and α = 45˚ on the chord.

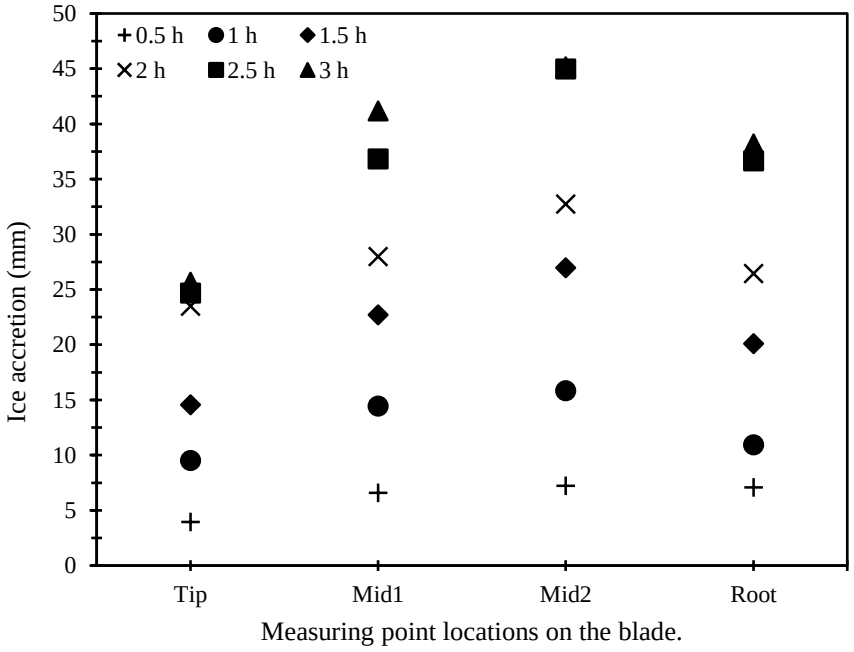

Figure 5:15: Ice accumulation for V = 3.5 m/s, θ = 45°, and α = 45˚ on the thickness.

Figure 5:16: Shape of ice accumulation on the blade at V = 3.5 m/s, θ = 45°, and α = 45˚.

The four points maintained their order as in the previous test (Test 4) with a slight difference in this test (Test 5) in terms of the amount of ice accumulation, as observed in Figure (5:17 and 5:18).

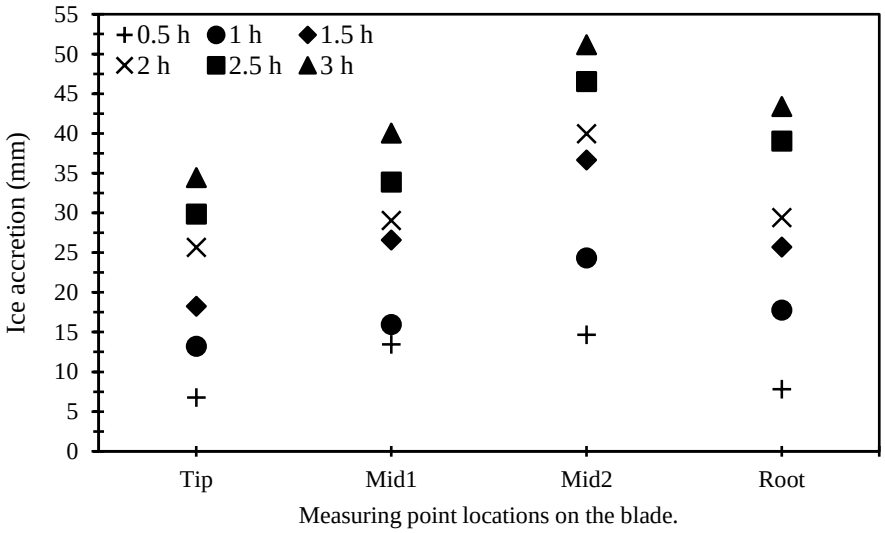

Figure 5:17: Ice accumulation for V = 4 m/s, θ = 45°, and α = 45˚ on the chord.

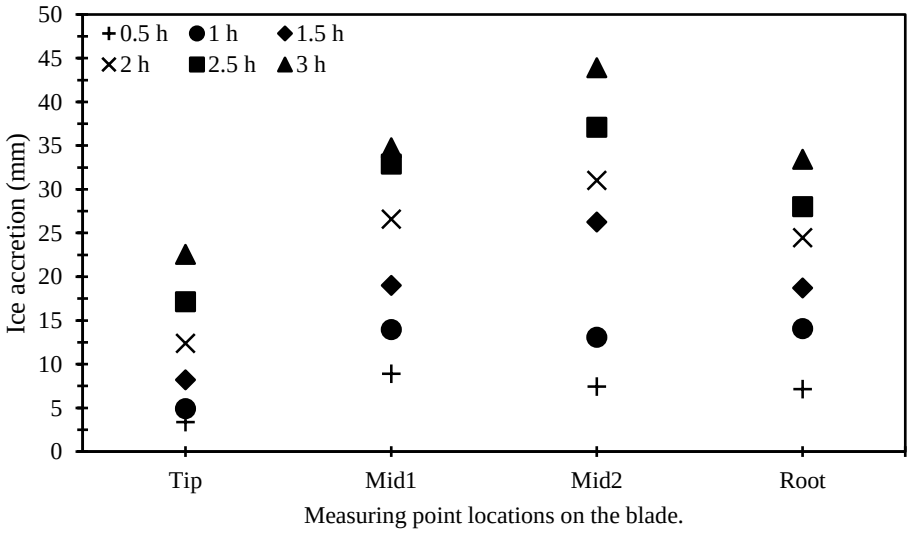

Figure 5:18: Ice accumulation for V = 4 m/s, θ = 45°, and α = 45˚ on the thickness.

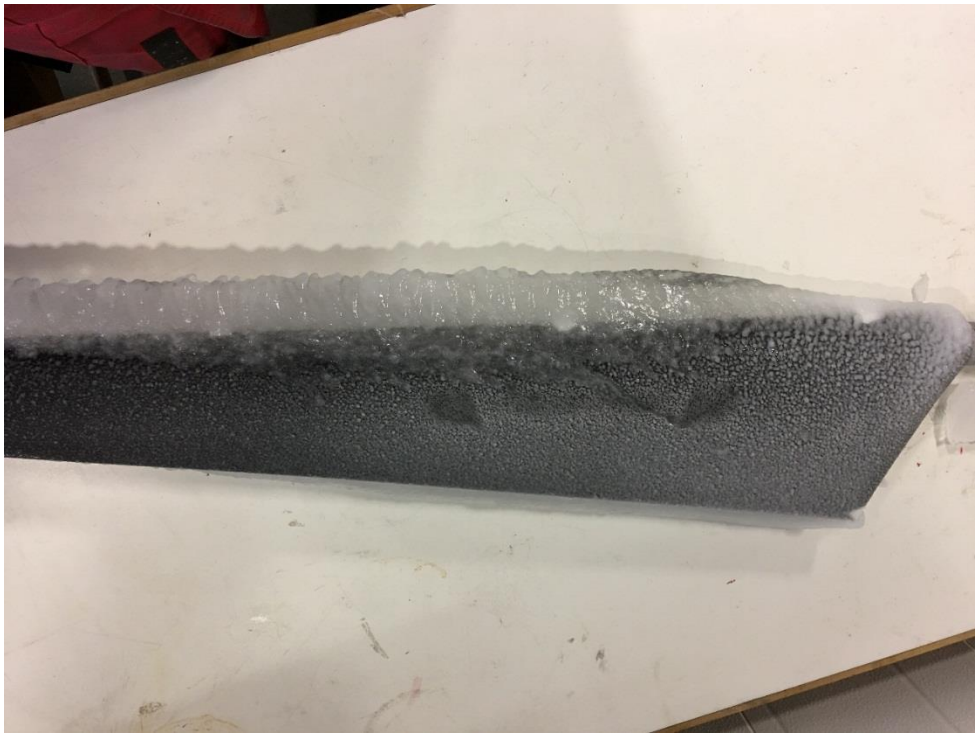

Figure 5:19: Shape of ice accumulation on the blade at V = 4 m/s, θ = 45°, and α = 45˚.

Test 6 was not different from its predecessors. The overall shape of the points is very similar to the previous test, with a clear difference in the amount of accumulation of ice. All results shown in Figures (5:20, 5:21 and 5:22).

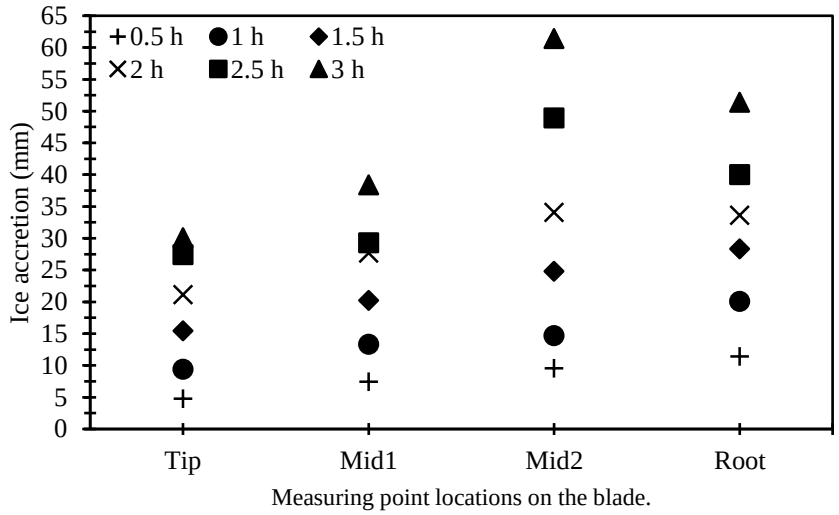

Figure 5:20: Ice accumulation for V = 5 m/s, θ = 45°, and α = 45˚ on the chord.

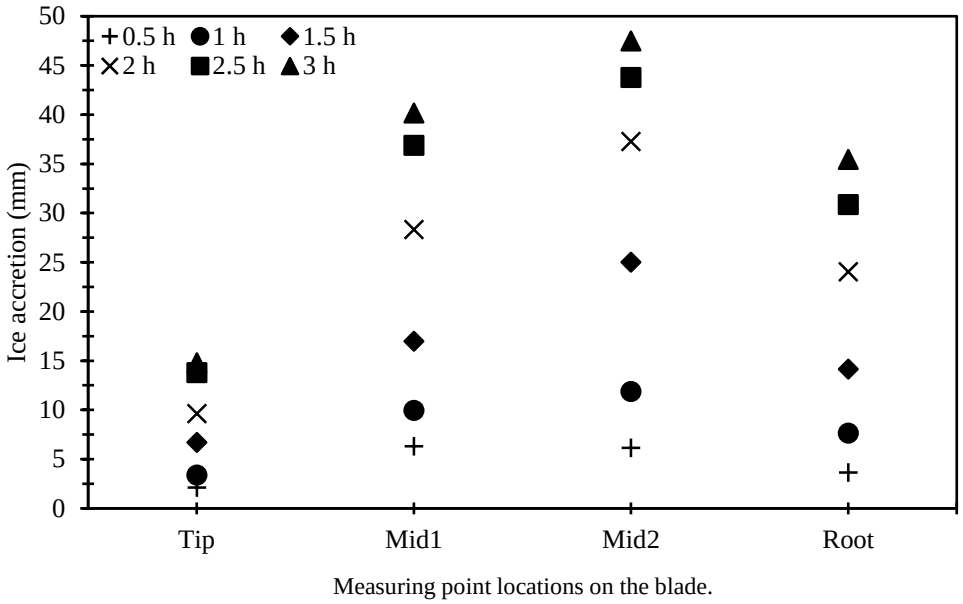

Figure 5:21: Ice accumulation for V = 5 m/s, θ = 45°, and α = 45˚ on the thickness.

Figure 5:22: Shape of ice accumulation on the blade at V = 5 m/s, θ = 45°, and α = 45˚.

In this position, with the blade placed at 45 degrees from the horizon, the results were not different from the previous results in terms of order. The weight of ice for Test 6 was the largest, followed by the Test 5 and, Test 4 (See Figure. 5:23). However, the weight was different from the previous results (Test 1, Test 2 and Test 3), where the amount was about 30% higher than in the first three tests.

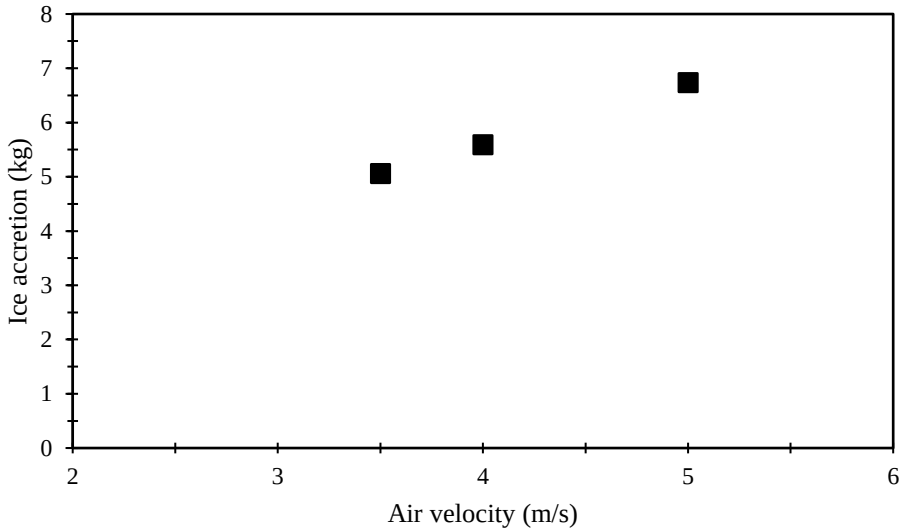

Figure 5:23: Weights of Ice accretion at θ = 45°, and α = 45°.

5.4 Blade at an Angular Position of $\theta = 90^{\circ}$ and $\alpha = 45^{\circ}$:

As shown in the Figure (5:24, 5:25 and 5:26), the overall appearance of the two figures is very similar, with a clear difference in ice accumulation. The highest point is Mid 1, then Mid 2 and the Tip, followed by the Root. Note that in figure (5:24) the difference between each point in the order is very similar. However, in figure (5:25), the points (Mid 2 and Tip) are roughly on the same line, indicating the same cumulative ice rate.

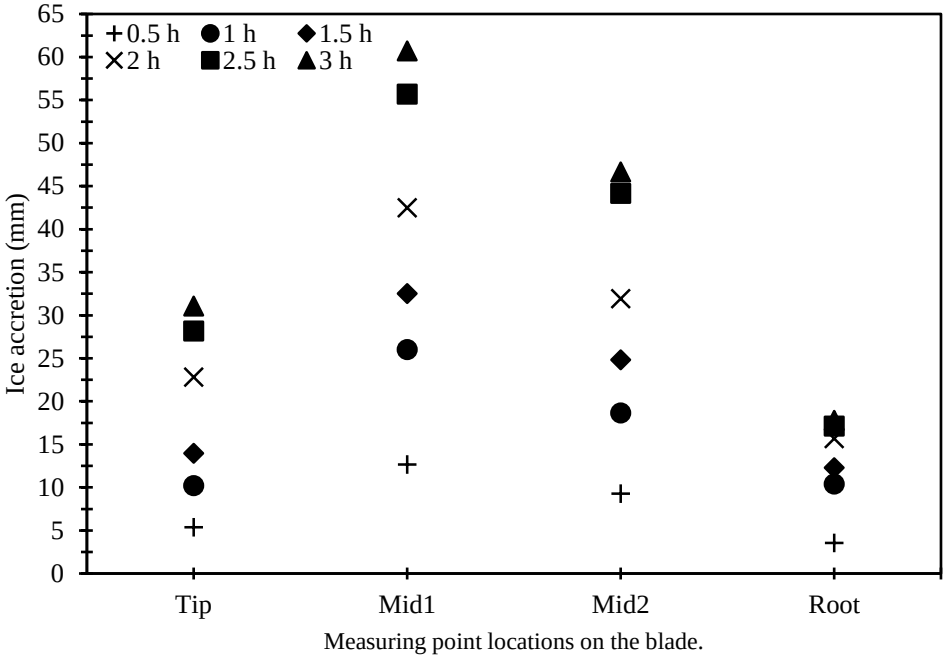

Figure 5:24: Ice accumulation for V = 3.5 m/s, θ = 90°, and α = 45˚ on the chord.

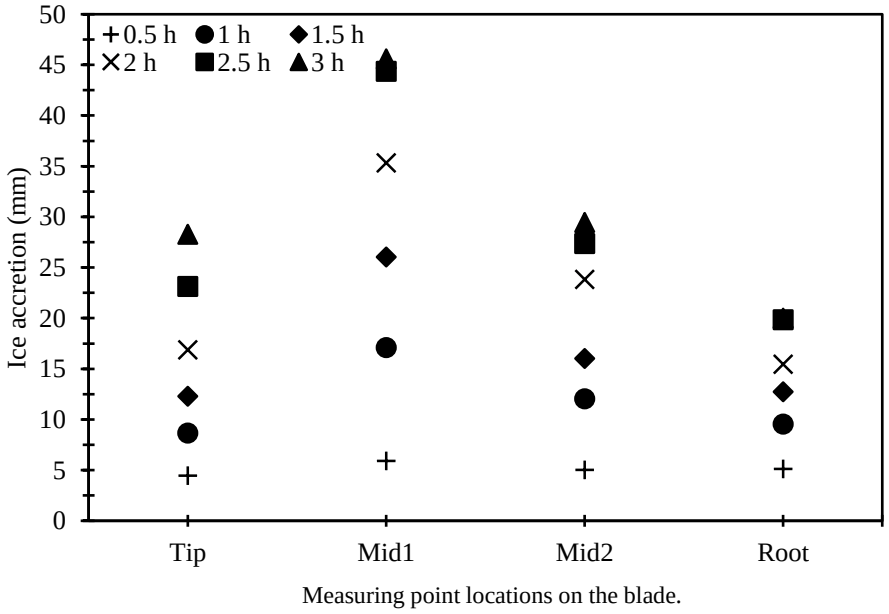

Figure 5:25: Ice accumulation for V = 5 m/s, θ = 45°, and α = 45˚ on the thickness.

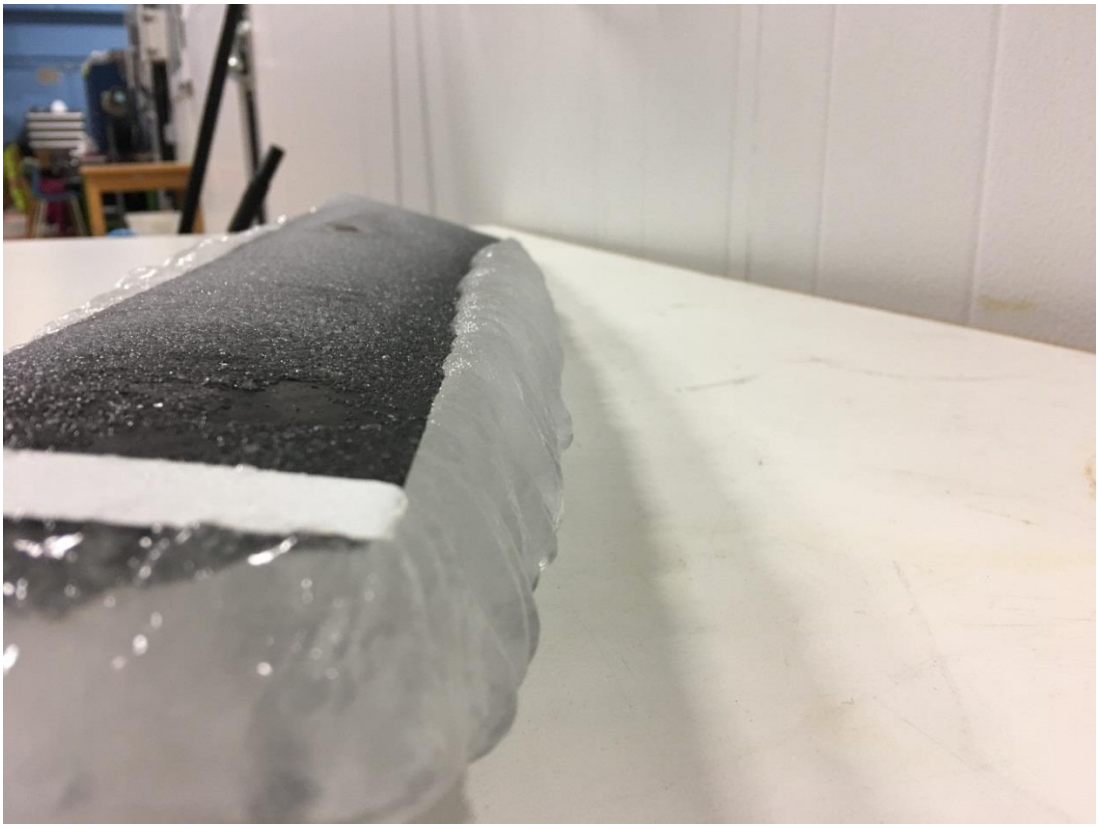

Figure 5:26: Shape of ice accumulation on the blade at V = 3.5 m/s, θ = 45°, and α = 45˚.

The general shape of Test 8 was not different from Test 7, but the Root, Tip, and Mid 2 were very similar to each other, as shown in figure (5:27), with a difference of order. The Tip was last and The Mid1 was the highest point, followed by Mid 2 and then the Root. However, figure (5:28) shows that the highest accumulation of ice was at the Mid1, then Mid 2, the Tip came third and the Root had the least accumulation. It was observed that the difference in accumulation of ice was clear between Mid 1 and Mid 2, with a slight difference between the three remaining points. See Figure (5:29).

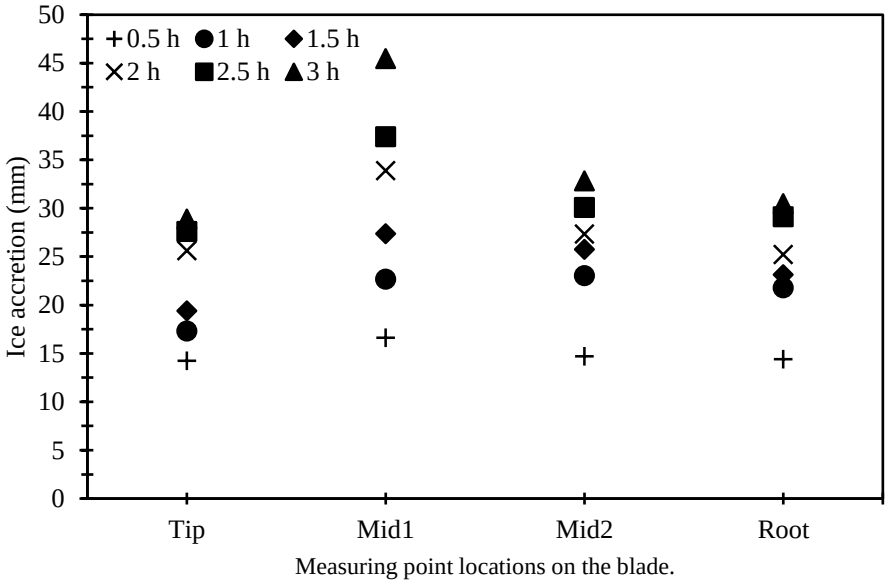

Figure 5:27: Ice accumulation for V = 4 m/s, θ = 90°, and α = 45˚ on the chord.

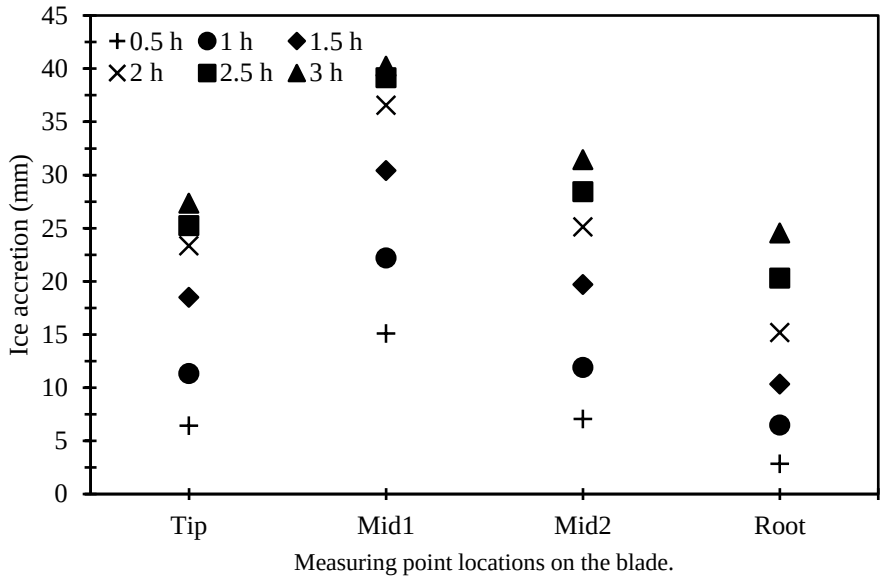

Figure 5:28: Ice accumulation for V = 4 m/s, θ = 90°, and α = 45˚ on the thickness.

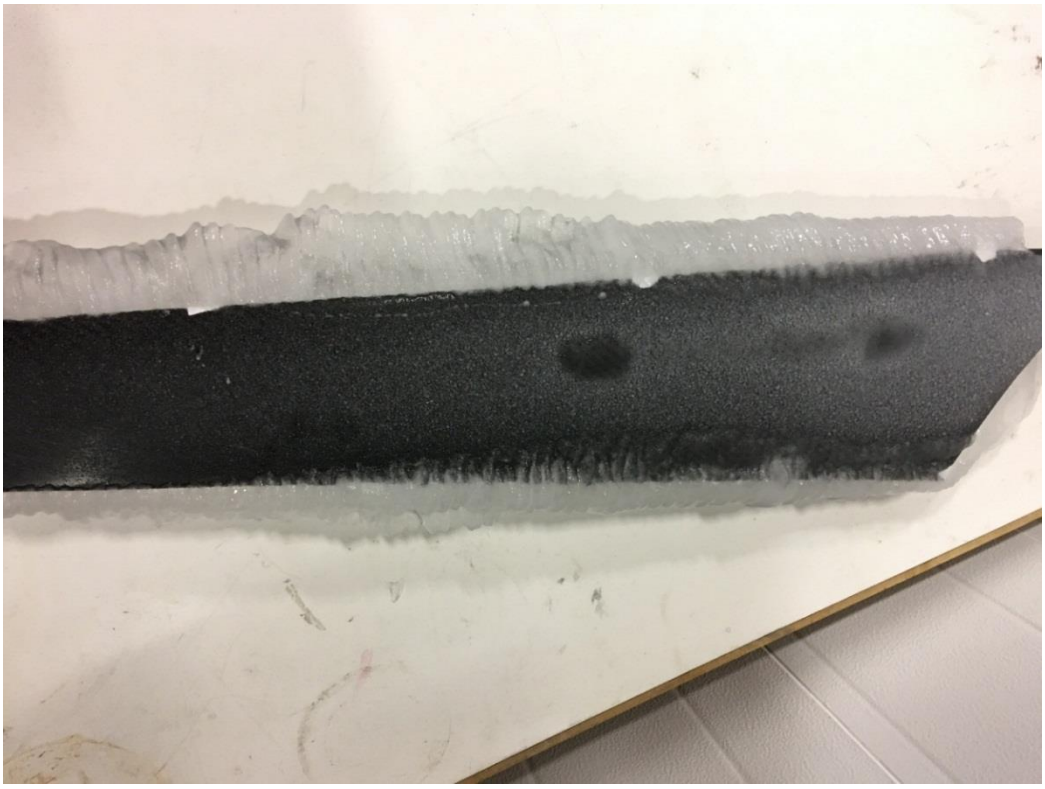

Figure 5:29: Shape of ice accumulation on of the blade at V = 4 m/s, θ = 90°, and α = 45˚.

As for the vertical position of the blade, the results were different from those expected. The most accumulation of ice was at the Mid 1 and then gradually reduced to the Root. The results were very close between the Tip and the Root at all speeds, and almost equal, as shown in Figure (5:30, 5:31 and 5:32).

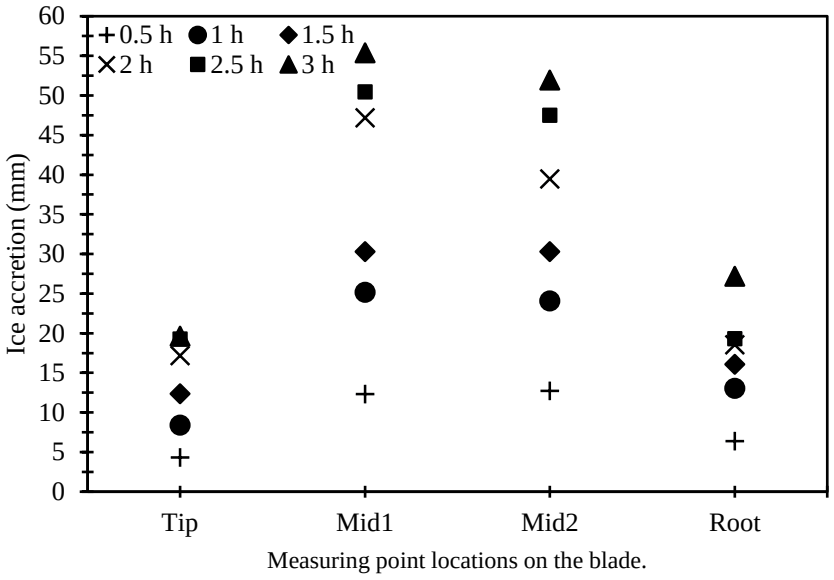

Figure 5:30: Ice accumulation for V = 5 m/s, θ = 90°, and α = 45˚ on the chord.

In addition, the results do not differ from the previous results in terms of ranking. However, the significant difference between Mid2 and the Root was observed and between Mid1 and the Tip. See Figure (5:34). However, the ranking was the same as the previous one. For Figure (5:35), the ranking was similar to Test 8 with an increase in the amount of ice accumulation.

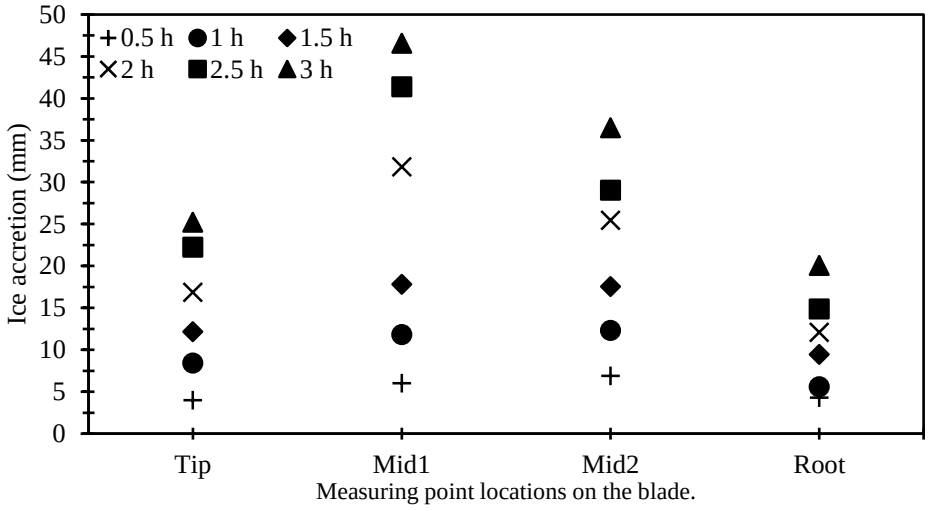

Figure 5:31: Ice accumulation for V = 5 m/s, θ = 90°, and α = 45˚ on the thickness.

Figure 5:32: Shape of ice accumulation on of the blade at θ = 90°, and α = 45˚.

Figure (5:33) shows that the highest accumulation of ice was in Test 9 followed by Test 8, and that the lowest amount of accumulation at Test 7. Note that the blade was placed vertically, but overall, the amount of ice was less than for the previous Tests (4, 5 and 6) by approximately 12%.

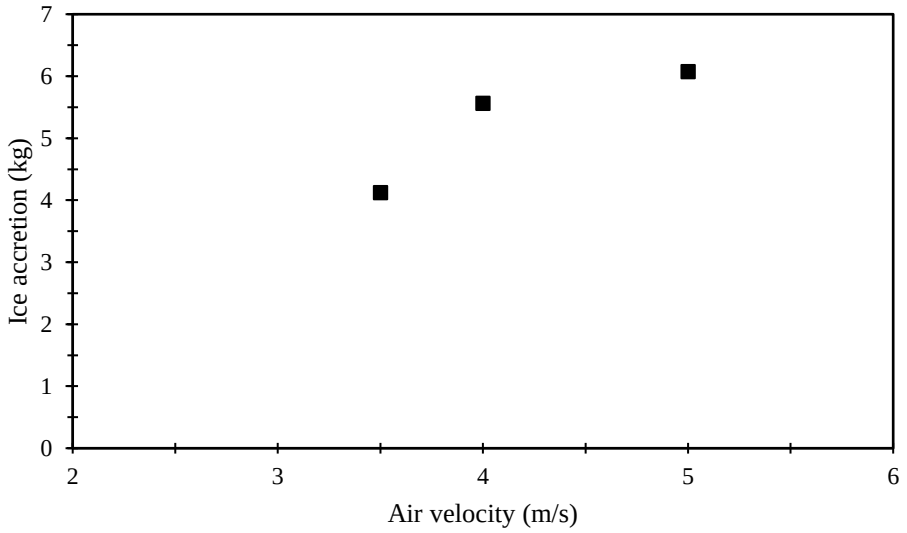

Figure 5:33: Weights of Ice accretion at θ = 90°.

5.5 Summary of previous Tests results:

In general, the results of the first three Tests (1, 2 and 3) indicated that the largest accumulation of ice was in the middle of the blade (Mid 1 and 2), and the lowest was at the extremities (Root and Tip). These results may have been affected by wind velocity. In Figuers. 5:1, 5:2 and 5:3, the wind speed was greater in the middle than at the sides, but the difference was not significant. These factors, wind speed and spray position were taken into account before the start of the experiment, and this was the most suitable position to experiment. However, in the following three Tests (4, 5 and 6), the results were quite different; the effect of the blade position was evident. More accumulation of ice occurred from the middle of the blade up to the root, which meant that the slope of the blade led to the water droplets heading towards the root. In addition, the cold air temperature affected the movement of water droplets as then reached the Mid 2 point and froze, making it the highest point of accumulation of ice. This position was the most complex position of the ice, as seen in Figure (5:34), at all different speeds.

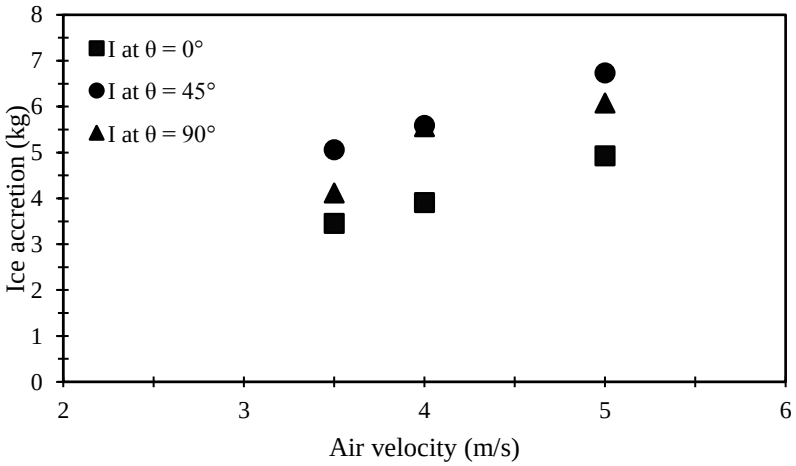

Figure 5:34: Weights of ice accumulation.

As for the position of the vertical blade, we see clearly the difference in ice weight at speed 3.5 with other positions. However, the results are approaching velocity 4 between the vertical position ($\theta = 90^{o}$) and 45 ° position ($\theta = 45^{o}$) of the blade.

The results as shown in (Fig. 5:35) are logical and predictable; the highest accumulation of ice is at the highest wind speed. Note that the results are close, at 3.5 and 4 (m/s) at 45° for the blade, and are spaced for the rest of the positions. However, the results for 4 and 5 (m/s) were spaced at position 45° and converged in the rest of the positions.

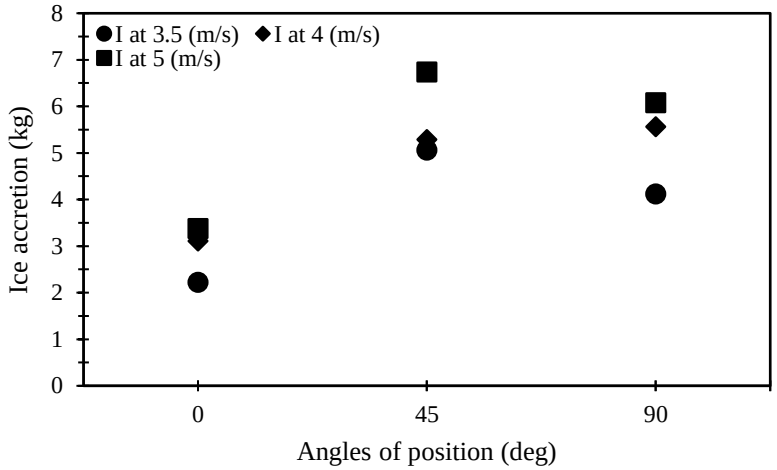

Figure 5:35: Weights of ice accretion.

5.6 Blade at an Angular Position of $\theta = 0^{\circ}$ and $\alpha = 0^{\circ}$:

In this case, I will change the angle of the attack (α**)** and the angle of the blade position will be constant (θ).

In Test 10, I note that the highest accumulation of ice was at the Mid 2 where the difference between it and the next point is clear, then the two points came in Mid 1 and Root in the second and the third respectively, and they were very close. See Figure (5:36).

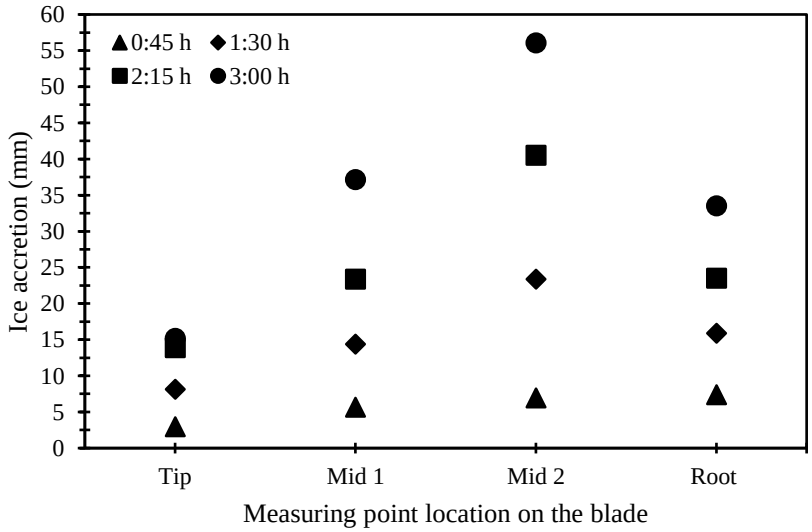

Figure 5:36: Ice accumulation for V = 5 m/s, θ = 0°, and α = 0˚ on the chord.

As for the accumulation of ice on the thickness of the blade, it is quite different from the accumulation of ice on the blade. Where the highest accumulation of ice was on the Mid 1 followed by the Mid 2 and then the Root. The difference was not large, but the difference was clear between them and the Tip. See Figure (5:37).

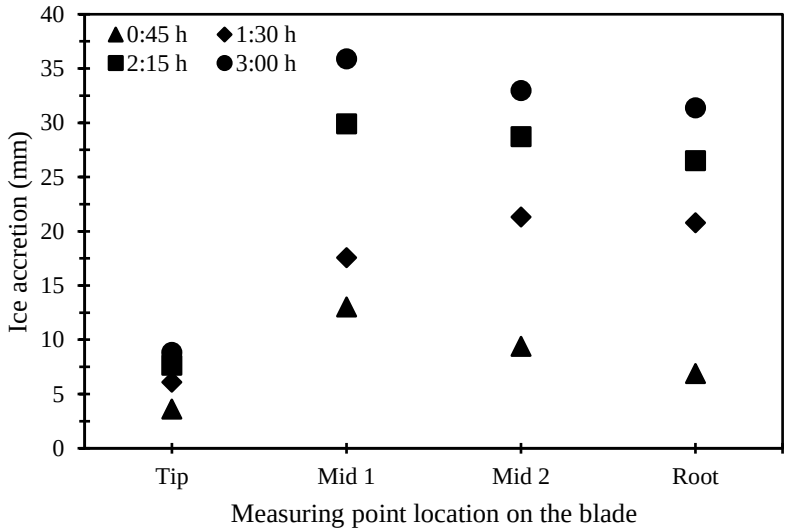

Figure 5:37: Ice accumulation for V = 5 m/s, θ = 0°, and α = 0˚on the thickness.

5.7 Blade at an Angular Position of $\theta = 0^{\circ}$ and $\alpha = 30^{\circ}$:

In this Test (11), the points came very close to each other except the Mid 2, where it was lower. The accumulation of ice was very close to almost equal to the three points (Mid 1, Root and Tip). I notice that the accumulation increased significantly after about an hour and a half. See Figure (5:38).

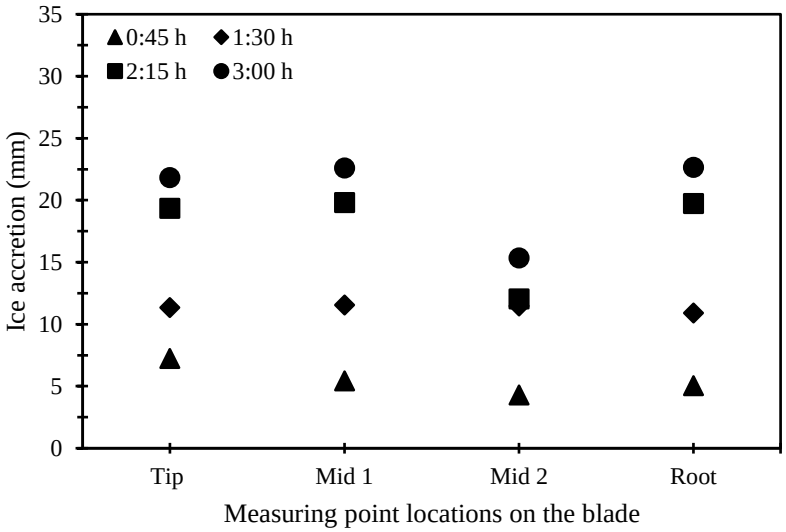

Figure 5:38: Ice accumulation for V = 5 m/s, θ = 0°, and α = 30˚ on the chord.

As for the accumulation of ice on the blade thickness, the highest accumulation was at the Mid 1 and then the Mid 2 and then the Root. The Tip came in the lowest ranking and a big difference between it and the three points. I also note that the accumulation of ice increased significantly after about an hour and a half from the beginning of the test. See Figure (5:39).

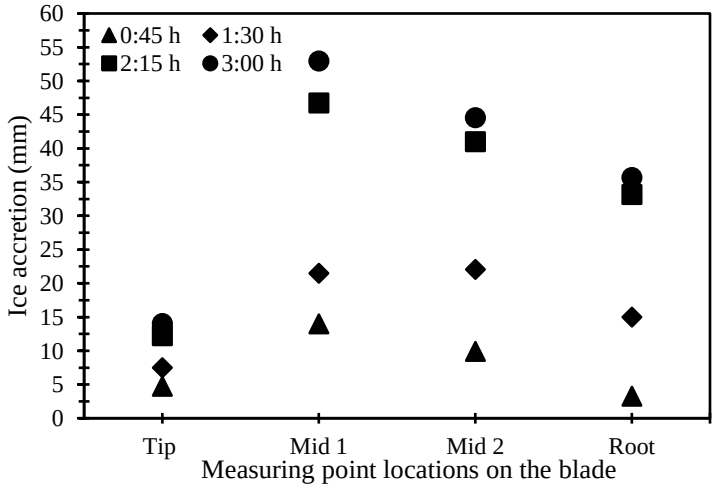

Figure 5:39: Ice accumulation for V = 5 m/s, θ = 0°, and α = 30˚ on the thickness.

5.8 Blade at an Angular Position of $\theta = 0^{\circ}$ and $\alpha = 60^{\circ}$:

The results were slightly different from the two previous tests in this Test (12). Where the highest point of accumulation of ice at the Mid 1 and then the Mid 2. However, I see a clear divergence of the ice accumulation between the edges of the blade (Root and Tip) and the middle of the blade (Mid 1 and Mid 2). See Figure (5:40).

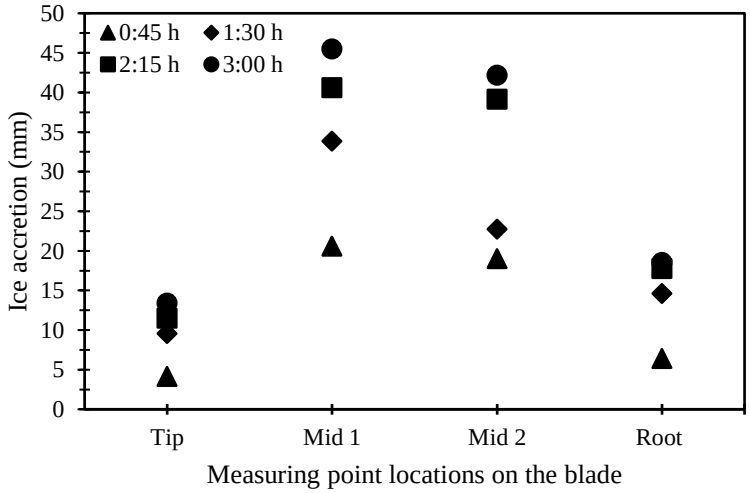

Figure 5:40: Ice accumulation for V = 5 m/s, θ = 0°, and α = 60˚ on the chord.

The accumulation of ice for the blade was logical, as the general shape was in the form of a pyramid where the top of the pyramid was at Mid 2 and the base was at the Root and the Tip. Where the points were close to each other and there was not much difference. See Figure (5:41).

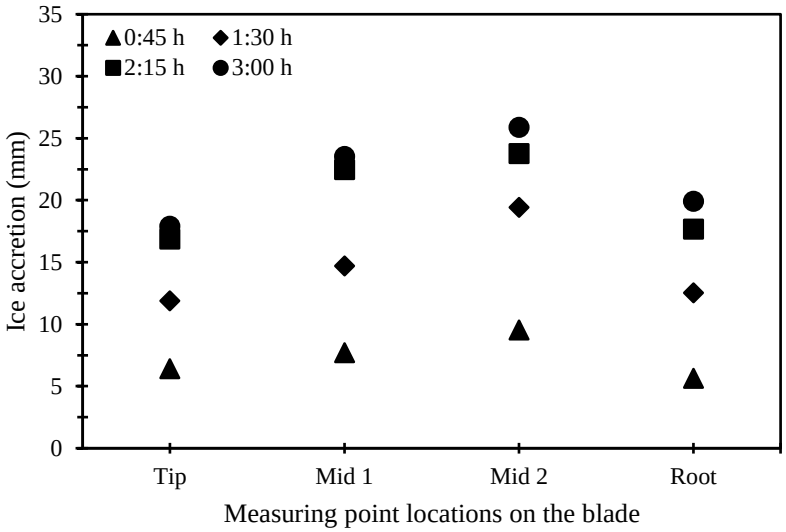

Figure 5:41: Ice accumulation for V = 5 m/s, θ = 0°, and α = 60˚ on the thickness.

5.9 Blade at an Angular Position of $\theta = 0^{\circ}$ and $\alpha = 90^{\circ}$:

In this Figure (5:42), the results which, about the chord case were not different from previous tests. Where the highest accumulation of ice at the Mid 2 and followed by the Mid 1. The accumulation of ice on the root and head of the blade is equal to each other; in general, all the points were accumulated close to each other, and I did not notice a clear difference between them.

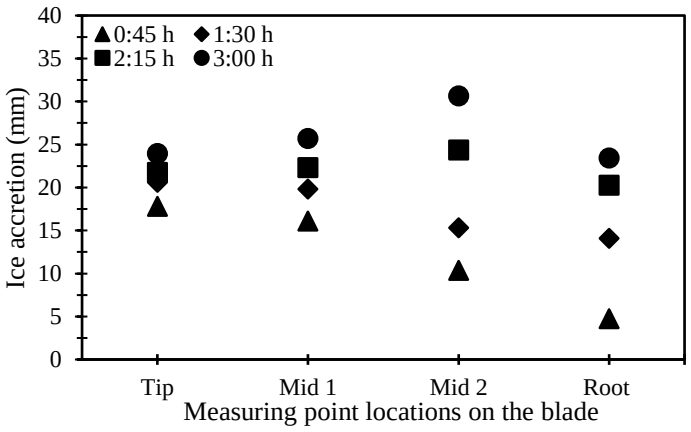

Figure 5:42: Ice accumulation for V = 5 m/s, θ = 0°, and α = 90˚ on the chord.

As for the accumulation of ice on the thickness of the blade, the order of the points was different from the accumulation of ice for the blade. Where the highest accumulation of ice was at the Mid 2 followed by the Root then the Mid 1 and the lowest accumulation was at the Tip. In addition, there is a clear difference between the first three points at 3 hours. See Figure (5:43).

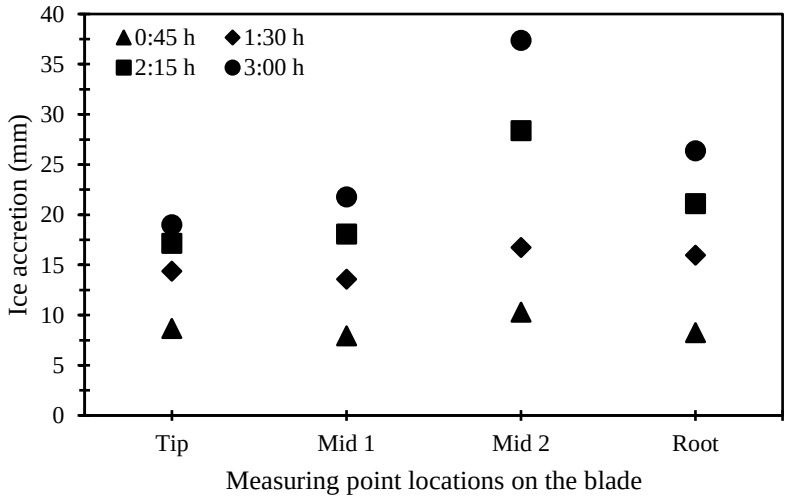

Figure 5:43: Ice accumulation for V = 5 m/s, θ = 0°, and α = 90˚ on the thickness.

The results of the ice weights were increased, where the highest ice weight was at the attack angle 90˚ and gradually reduced to the lowest ice weight at the attack angle 0˚. This rise in ice weight is logical as the area facing the flow increases as the angle of attack increases. Therefore, it is normal to increase the amount of ice accumulation on the blade, which increases the weight of the ice (See Figure 5:44).

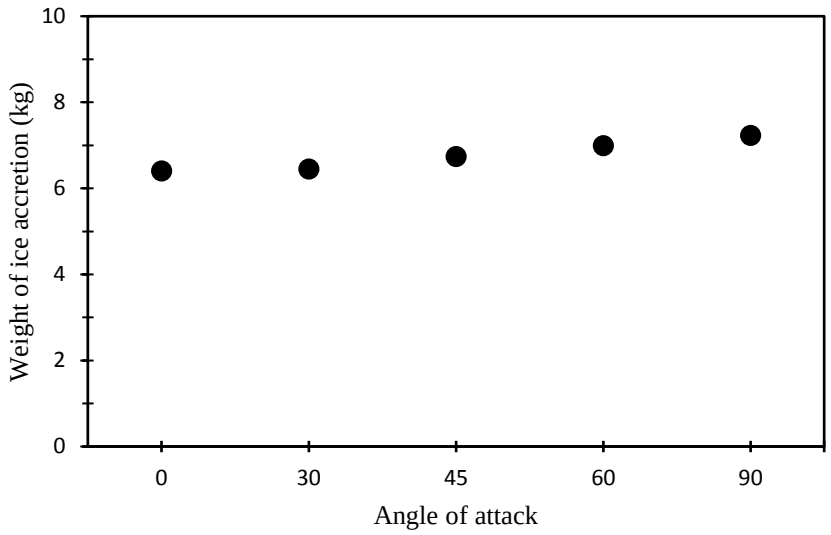

Figure 5:44: Weight of ice at different angle of attack (α).

5.10 Comparing of the results:

In this section, I will compare the results with each other according to the situation. All situations will be at (t =3 h).

5.10.1 Comparing the results of ice accumulation at $\alpha = 45^{\circ}$ and $\theta = 45^{\circ}$.

In Figure (5:45), I observe that the overall shape of the points is similar with the difference in ice accumulation. The highest accumulation of ice at the highest speed of wind (5 m/s) was at the Mid 2. I also note that the ice accumulation rate has increased with increasing wind speed. The increase was almost equal at all measurement points. This confirms that the accumulation of ice has a direct relationship with the speed of the wind.

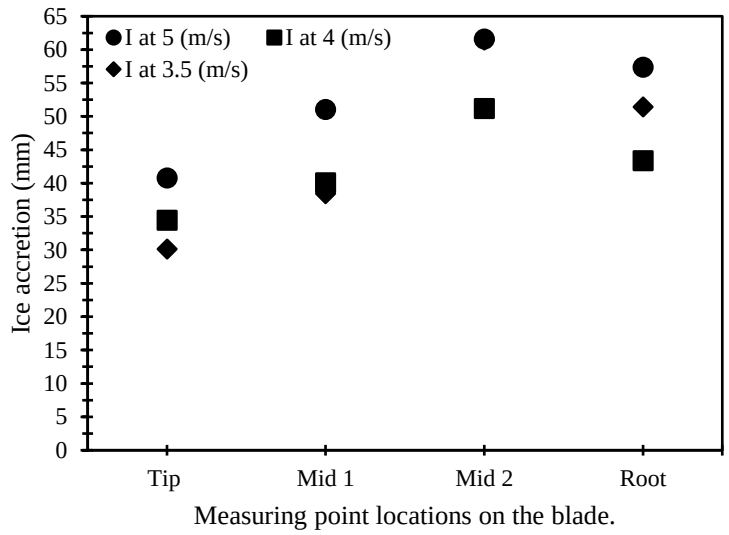

Figure 5:45: Ice accumulation at (t = 3 h), α = 45° and θ=45° on the chord.

As for the accumulation of ice on the thickness of the blade, it was different from the accumulation of ice on the chord. The highest accumulation of ice was at the midpoint 2 but at the lowest speed of the wind (3.5 m / s). In general, however, the overall shape of the accumulation points is very similar to the accumulation of ice on the chord. See Figure (5:46).

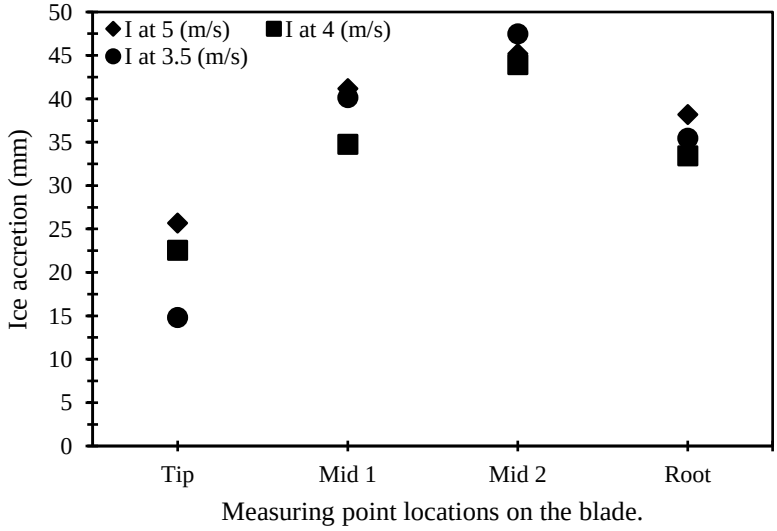

Figure 5:46: Ice accumulation at (t = 3 h), α = 45˚ and θ= 45˚ on the thickness.

In general, the results were fairly close to expectations. Where the Mid 2 was the highest point of ice accumulation, although the highest wind speed was at Mid 1 but here I believe that gravity has an effect on accumulation as well as the form of the blade.

5.10.2 Comparing the results of ice accumulation at $\alpha = 45^{\circ}$ and $\theta = 90^{\circ}$.

At all different speeds of the wind, Mid 1 was the highest point of ice accumulation, but the order of points is equal at the three speeds of wind. Here the effect of wind speed is clear, as the wind speed is high at the Mid 1; therefore, the ice accumulated at the Mid 1 even though the blade position was vertical. Expectations were that the highest ice accumulation would be at the Root, but the experiment proved that wind speed had an effect on ice accumulation greater than gravity. See Figure (5:47).

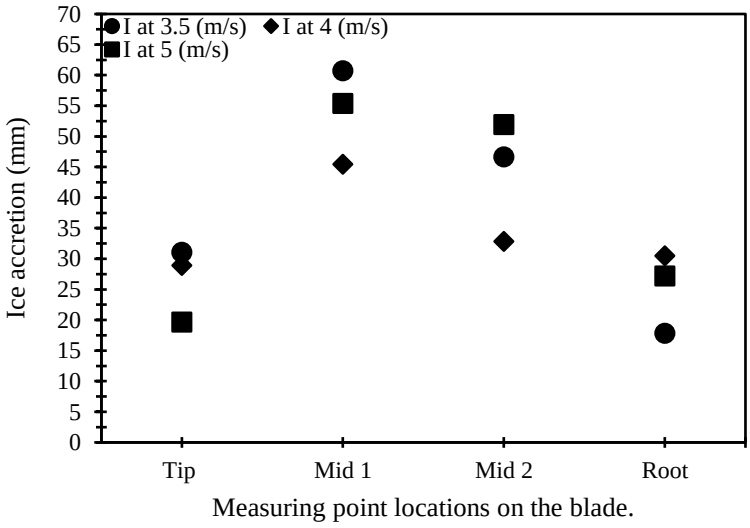

Figure 5:47: Ice accumulation at (t = 3 h), $\alpha = 45^{\circ}$ and $\theta = 90^{\circ}$ on the chord.

However, for the accumulation of ice on the thickness of the blade, the highest accumulation at the highest speed of the wind, which was at the point of Mid 1. In

addition, the shape of the blade affects the accumulation of ice in terms of the thickness, the chord and the angle of twist of the blade. See Figure (5:48).

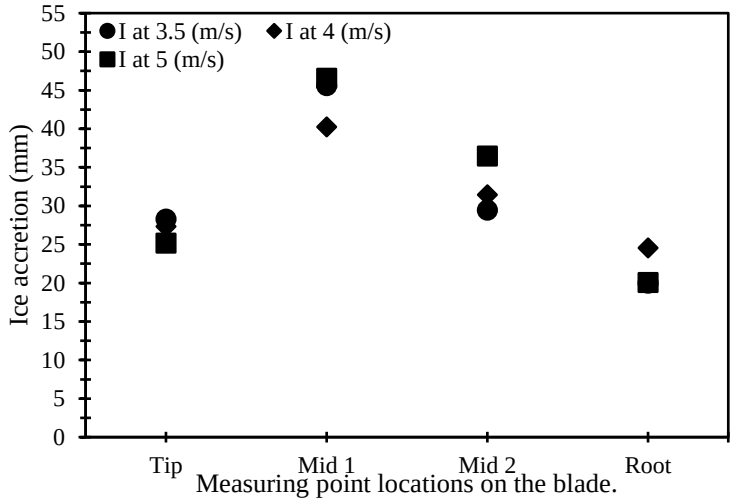

Figure 5:48: Ice accumulation at (t = 3 h), α = 45˚ and θ=90˚ on the thickness.

5.10.3 Comparing the results of ice accumulation at $\alpha = 45^{\circ}$ and $\theta = 0^{\circ}$.

In this case, the accumulation of ice was consistent with the wind speed, where the highest point of accumulation of ice at the Mid 1. All points were close to each other with a slight difference. See Figure (5:49).

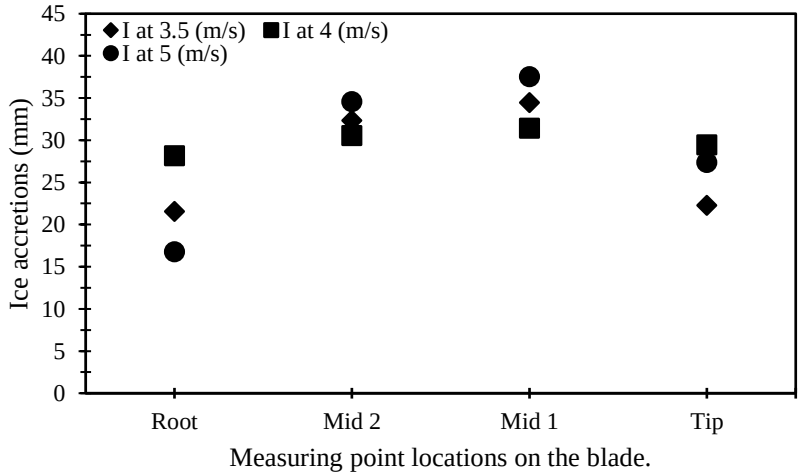

Figure 5:49: Ice accumulation at (t = 3 h), α = 45˚ and θ = 0˚ on the chord.

As for the accumulation of ice on the thickness of the blade, the highest accumulation happens at the Mid 1, but the general shape is different from the accumulation of ice on the blade. I noticed a clear difference between the four points especially between the Mid 2 and the Root and between the Mid 1 and the Tip. The effect of wind velocity was evident on the accumulation of ice on the thickness of the blade. See Figure (5:50).

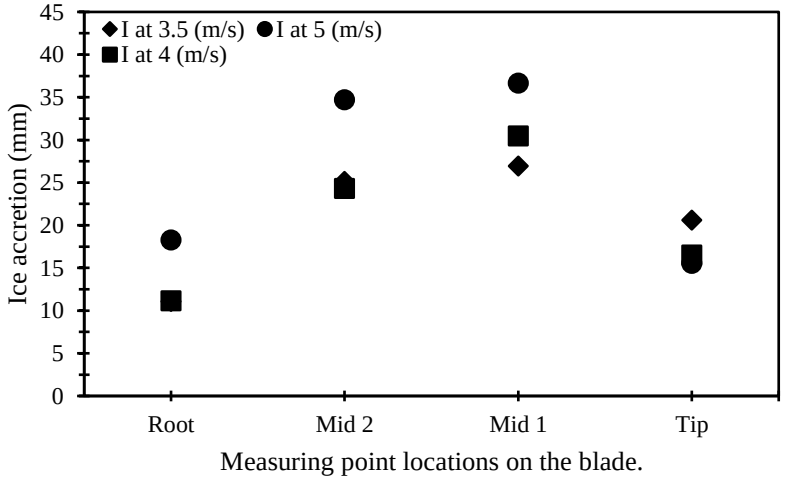

Figure 5:50: Ice accumulation at (t = 3 hr), α = 45˚ and θ=0˚ on the thickness.

` When comparing experimental data with the theoretical values, then the relative error is given by a similar formula:

$$\text{Relative error} = \left(\frac{\text{Experimental value} - \text{theoretical vlaue}}{\text{theoretical value}}\right) \times 100\% \qquad (5.1)$$

In this case, when applying this equation on the weight of ice accumulation of the three first tests, will get relative error for each test. Where relative error1 =5.8%, relative error 2= 2.59% and relative error 3 =3.71%. The theoretical values were measured through ice accretion model 1 Eq. 2.1.

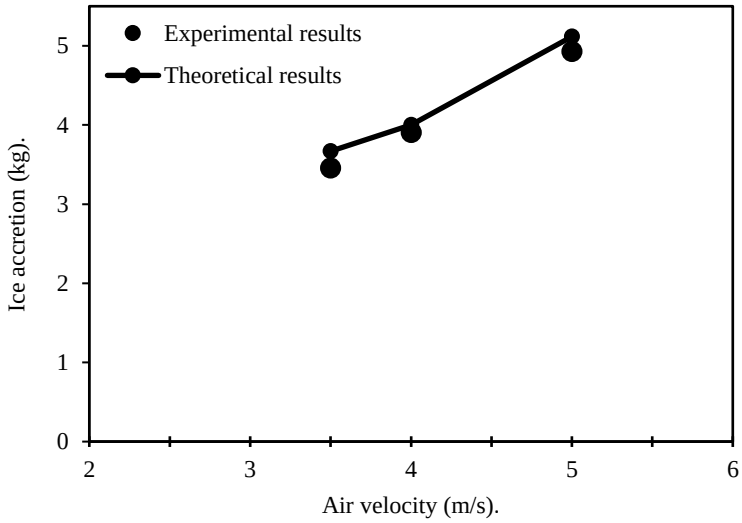

Figure 5:51: Comparing the experiment and theory results of weight of ice at $\alpha = 45^{\circ}$ and $\theta = 0^{\circ}$.

5.11 Experimental uncertainties

In this thesis, several measuring tools were used to obtain the results. As we know each measuring device that has a precision rate: the accuracy of the digital venire caliper is ±0.02 (mm) and the wind speed sensor is ±0.02 (m/s). Standard division applied on wind speed data and it is shown on Figure (5:52).

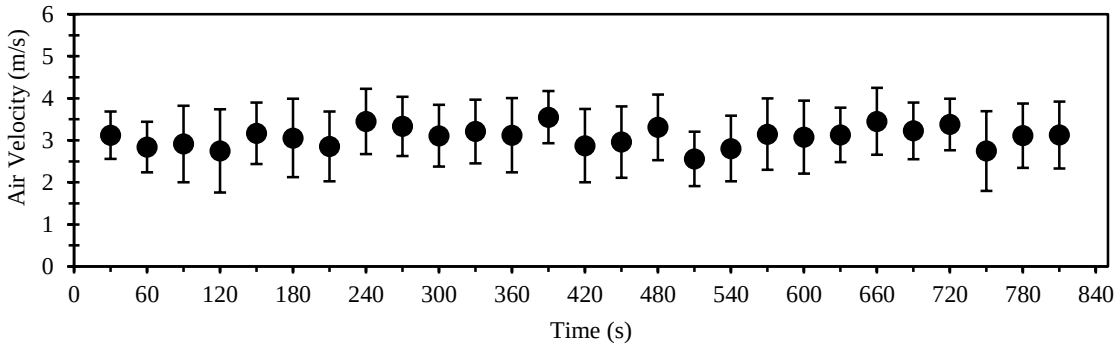

Figure 5:52: Wind speed with standard division at Root (45Hz).

This Figure (5:52) shows the wind speed at the root point when the fan is at 45 Hz, where the average speed was about 3.08 m / s. In the Appendix, there is a figure for each speed at each measurement point.

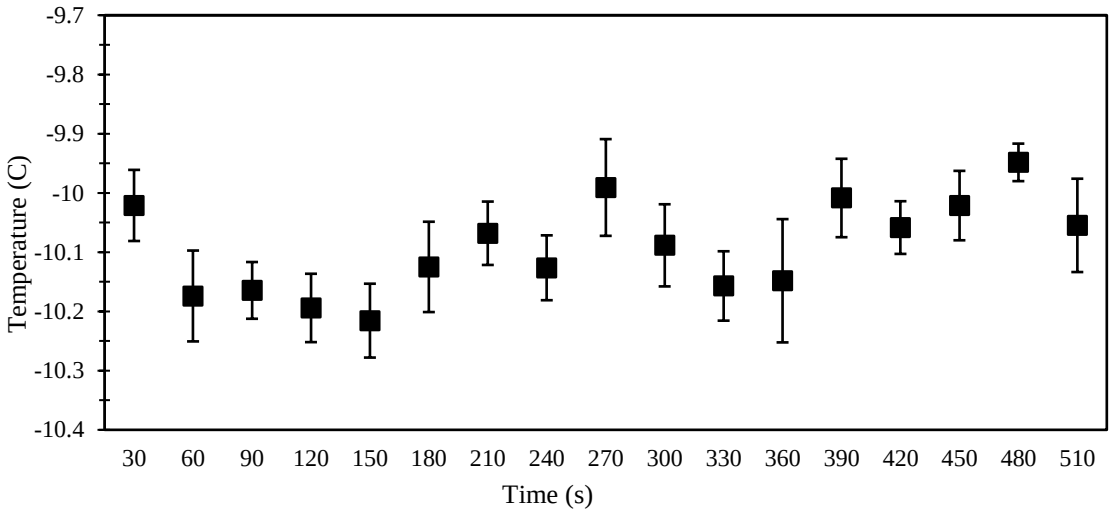

Figure 5:53: Temperature measurement during the test.

This Figure (5:53) shows the temperature during the test inside the cold chamber. For each test temperature, readings are shown as a figure, which is also placed in the appendix.

In order to verify the results, I performed one test twice and the test was at (α = 45˚ and θ = 0˚). I analyzed the results together by taking the average for each recording and its standard deviation both the chord and the thickness of the blade. See Figure (5:54).

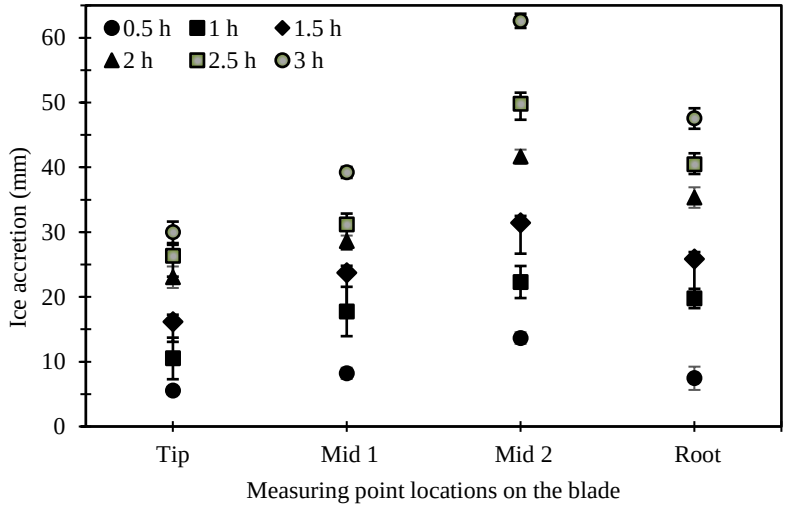

Figure 5:54: Average ice accumulation with standard deviation for V = 5 m/s, θ = 45°, and α = 45˚ on the chord.

In addition, it was also observed that recordings at 3 hours have a very low standard deviation. This proves that when the time of the experiment increases, its accuracy increases and this is seen in both cases (the thickness and the chord).

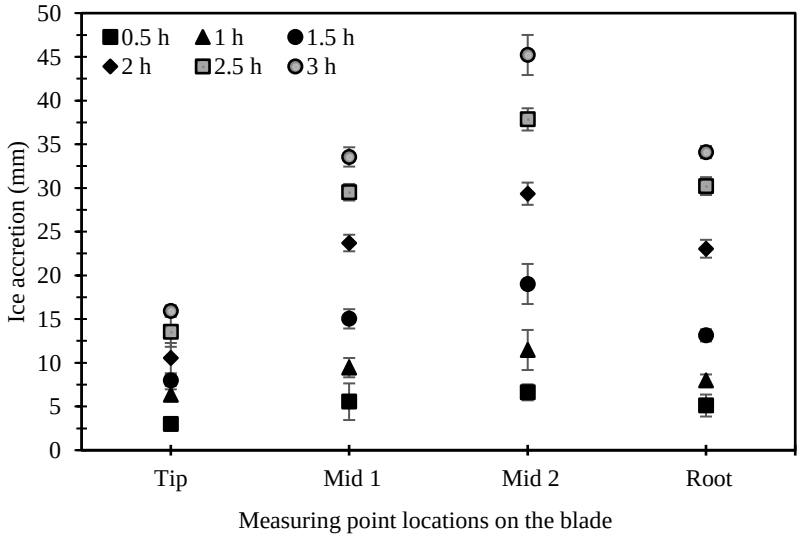

Figure 5:55: Average ice accumulation with standard division for V = 5 m/s, θ = 45°, and α = 45˚ on the thickness.

6. Chapter - Conclusion and Recommendations for Future Work

6.1 Conclusion

This thesis studied the accumulation of ice and its weight on the wind turbine blade, where the study was conducted on three different positions (horizontal, 45˚ and vertical) of the blade and three different speeds of wind (3.5, 4 and 5) m/s. Therefore, other parameters in the experiment were the temperature at -10 °C and LWC 0.6 g/m^3 at all experimental stages. The basic units were used to measure thickness and weight mm and kg respectively, because of there are common measurement tools. The experiment showed several results that can be summarized in the following points:

- Maximum ice accumulation on the chord of the blade was at (V = 5 m/s, θ = 45°, and α = 45˚) at Mid 1 point where it was about 61.41 mm.
- Maximum ice accumulation on the thickness of the blade was at (V = 5 m/s, θ = 45°, and α = 45˚) too at Mid 2 point where it was about 47.47 mm.
- Maximum weight of ice accretion on the blade was at (V = 5 m/s, θ = 45°, and α = 45˚) where it was about 6.734 kg.
- Minimum ice accumulation on the chord of the blade was at (V = 4 m/s, θ = 0°, and α = 45˚) at Mid 1 point where it was about 31.43 mm.
- Minimum ice accumulation on the thickness of the blade was at (V = 3.5 m/s, θ = 0°, and α = 45˚) at Mid 1 point where it was about 26.94 mm.
- Minimum weight of ice accretion on the blade was at (V = 3.5 m/s, θ = 0°, and α = 45˚) where it was about 3.455 kg.

Of these points, I note that the greatest accumulation of ice was at 5 m/s and -10 C˚, and the blade was at 45 degrees. Therefore, these parameters produced the highest accumulation of ice on the chord and the thickness of the blade and recorded the highest weight of ice. In addition, the least ice accumulation was at 3.5 m/s, -10 C˚ and the blade was horizontal. This means that position of the blade at 45˚ gives the water droplets more space to run on the blade surface until freezing as the droplets are carried along the blade. On the other hand, the horizontal position of the blade gives the droplets to run on the width of the blade, where I know that the width of the blade is less than the length, which led to the accumulation of ice less on the horizontal position of the blade. In addition, changing the attack angle of the wind led to an increase in ice accumulation as observed in the previous chapter. Because, changing the angle of attack increases the area facing the flow leading to increased ice accumulation.

6.2 Recommendations and Future Work

To improve the study of ice accumulation on the wind turbine blade I have considered some points for future studies:

- The rotation of the wind turbine blade during the test has an effect on the accumulation of ice on the blade of the turbine. I, therefore, recommend it in future studies.
- The existence of a wind tunnel during the test adjusts the wind speed corresponding to the blade and gives more precise and reliable results.

References

Ahti, K. “Ice load forecasts in Finland,” BOREAS VII, Saariselka, Finland. 7-8 March, 2005.

Alsabagh, A., Tiu, W., Xu, Y., & Virk, M. (2013). A Review of the Effects of Ice Accretion on the Structural Behavior of Wind Turbines. Wind Engineering, 37(1), 59-70.

Antonini, C., Innocenti, M., Horn, T., Marengo, M., & Amirfazli, A. (2011). Understanding the effect of super hydrophobic coatings on energy reduction in anti-icing systems. Cold Regions Science and Technology, 67(1), 58-67.

Barber, S., Wang, Y., Chokani, N., and Abhari, R. S. (2009). The effect of ice shapes on wind turbine performance. In 13th Int. Workshop on Atmospheric Icing, Andermatt, Switzerland.

Brodkey, R.S., Hershey, H.C., 1988. Transport phenomena: a unified approach. McGraw International Edition, New York (847 pp.).

Burton, T., Jenkins, N., Sharpe, D., & Bossanyi, E. (2011). Wind energy handbook. John Wiley & Sons.Boyle, G. (2004). Renewable Energy. Oxford University Press.

Canada Wind Energy Association. (2015). *Wind energy market/ Installed capacity.* Retrieved from http://canwea.ca/wind-energy/installed-capacity/.

Chaîné, P.M., et al. Wind and ice loading in Canada, 1974. Toronto: Atmospheric Environment Canada, 1974.

Dobesch, H., Nikolov, D. and Makkonen, L., 2005, “Physical processes, modelling and measuring icing effects in Europe”, Oesterr.Beitr.zu Meteorologie und Geophysik, no 34.

Fikke, S. (2006). Cost 727-Atmospheric icing on structures; measurement and data collection on icing. State of the Art. MeteoSwiss.

Finstad, K. and Lozowski, E., 1988, “A computational investigation of water droplet trajectories”, Journal of atmospheric and oceanic technology, vol. 5, pp. 160-170.

Finstad, K., Lozowski, E. and Makkonen, L., 1988b, “On the median volume diameter approximation for droplet collision efficiency”, Journal of the atmospheric sciences,

vol. 45, no. 24, pp. 4008-4012.

Fortin, G., Perron, J., Ilinca, A., 2005. Behaviour and Modeling of Cup Anemometers under Icing Conditions, IWAIS XI, Montréal, Canada, p. 6.

Frohboese, P., & Anders, A. (2007). Effects of icing on wind turbine fatigue loads. In Journal of Physics: Conference Series (Vol. 75, No. 1, p. 012061). IOP Publishing.

Gent, R.W., Dart, N.P., Cansdale, J.T., 2000. Aircraft icing. Philosophical Transactions of the Royal Society of London.

Haaland, S. S. (2011). Estimating Production Loss due to Icing on Wind Turbines (Master's thesis, Italy/University of Troms, 2011). Energy, Climate and Environment.

Hansen, A. C., & Butterfield, C. P. (1993). Aerodynamics of horizontal-axis wind turbines. Annual Review of Fluid Mechanics, 25(1), 115-149.Holdo, A.E.,

Mayman, P., Lun, I., Calay, R.K., 1997. Experimental simulation of runback ice. Journal of aircraft.

Homola, M. C., Ronsten, G., and Nicklasson, P. J. (2009). Energy production losses due to iced blades and instruments at Nygardsfjell, Sveg and Aapua. In 13th International workshop on Atmospheric Icing.

Homola, M.C., Nicklasson, P.J., Sundsbo, P.A., Virk, M.S., Wallenius, T., 2010. Effect of atmospheric temperature and droplet size variation on ice accretion of wind turbine blades. Journal of Wind Engineering and Industrial Aerodynamics.

Homola, M., Nicklasson P., and Sundsbø, P., 2006, "Ice sensors for wind turbines", Cold Regions Science and Technology, vol. 46, pp. 125-131

ISO 12494, 2001, Atmospheric icing on structures. Ref nr: ISO 12494:2001(E).

Jasinski, W. J., Noe, S. C., Selig, M. S., and Bragg, M. B. (1998). Wind turbine performance under icing conditions. Journal of Solar Energy Engineering, 120(1):6.

Kraj, A. G., & Bibeau, E. L. (2010). Measurement method and results of ice adhesion force on the curved surface of a wind turbine blade. Renewable Energy, 35(4), 741-746.

Laakso, T., Tallhug, L., Ronsten, G., Cattin, R., Baring- Gould, I., Lacroix, A., Peltola, E., Wallenius, T., and Durstewitz, M. (2009). Wind energy in cold climate idea task 19 outlook 2010. In 13th Int. Workshop on Atmospheric Icing, Andermatt, Switzerland.

Laakso, T., et al., 2003. State-of-the-art of wind energy in cold climates. IEA Wind Annex XIX, p. 53.

Laforte, JL., Allaire, M.A., 1992. Évaluation du Givromètre d'Hydro-Québec à Différentes Intensités de Givrage Sec et Humide. Rapport HQ-92-02.

Langmuir, I. and Blodgett, K., 1946, "A mathematical investigation of water droplet trajectories", Collected works of Irving Langmuir, vol. 10, pp.335-393, Oxford Pergamon press.

Marjaniemi, M., Peltola, E., 1998. Blade Heating Element Design and Practical Experiences, BOREAS IV. FMI, Hetta, Finland, pp. 197–209.

Makkonen, L., Lakso, T., Marjaniemi, M., and Finstad, K. J. (2001). Modeling and prevention of ice accretion on wind turbines. Wind engineering, 25:3{21}.

Makkonen, L., 1984, "Heat transfer and icing of a rough cylinder", *Cold Regions Science and Technology*, vol. 10, pp. 105-116.

Makkonen, L., 2000, "Models for the growth of rime, glaze, icicles and wet snow on structures", Philosophical Transactions of the Royal Society, vol. 358, pp. 2913-2939.

Manwell, J., McGowan, J., and Rogers, A. (2002). Wind Energy explained: Theory, Design and Application, chapter 3, page 84. John Wiley & Sons, Ltd, Chichester, UK.

Manwell, J. F., McGowan, J. G., & Rogers, A. L. (2010). Wind energy explained: theory, design and application, chapter 1, page 4-10. John Wiley & Sons, Edition.

Manwell, J. F., McGowan, J. G., & Rogers, A. L. (2010). Wind energy explained: theory, design and application, chapter 3. John Wiley & Sons, Edition

Mazin, I.P., Korolev, A.V., Heymsfield, A., Isaac, G.A., Cober, S.G., 2001. Thermodynamics of icing cylinder for measurements of liquid water content in supercooled clouds. J. Atmos. Ocean. Technol. 18, 543–558.

Parent, O., & Ilinca, A. (2011). Anti-icing and de-icing techniques for wind turbines: Critical review. Cold regions science and technology, 65(1), 88-96.

Rindeskär, E. (2010). Modelling of icing for wind farms in cold climate (Master's thesis, Uppsala universitet, 2010) (pp. 3-5). Uppsala: Uppsala university. doi:1650-6553.

Ronsten, G., Dierer, S., Nygaard, B., Makkonen, L. and Homola, M., 2009, "Measures needed for the successful development of wind energy in icing climates", retrieved from http://www.ewec2009proceedings.info/allfiles2/661_EWEC2009presentation.pdf, 090311.

Seifert, H. and Richert, F. (1998). A recipe to estimate aerodynamics and iceloads on iced rotor blades. In BOREAS IV, Hetta, Finland. Enontekiö.

Shin, J., Berkowitz, B., Chen, H., Cebeci, T., 1991. Prediction of ice shapes and their effect on airfoil performance, NASA Technical Memorandum.

Tammelin, B. and Seifert, H. (2001). Large wind turbines go into cold climate regions. In EWEC 2001. Copenhagen.

Walton, W.H., Woolcock, A., 1960. The suppression of airborne dust by water spray. Int. J. Air Pollut. 3, 129–153.

Øyvind Byrkjedal. (2009). Estimating wind power production loss due to icing. In 13th Int. Workshop on Atmospheric Icing, Andermatt, Switzerland.

Appendix

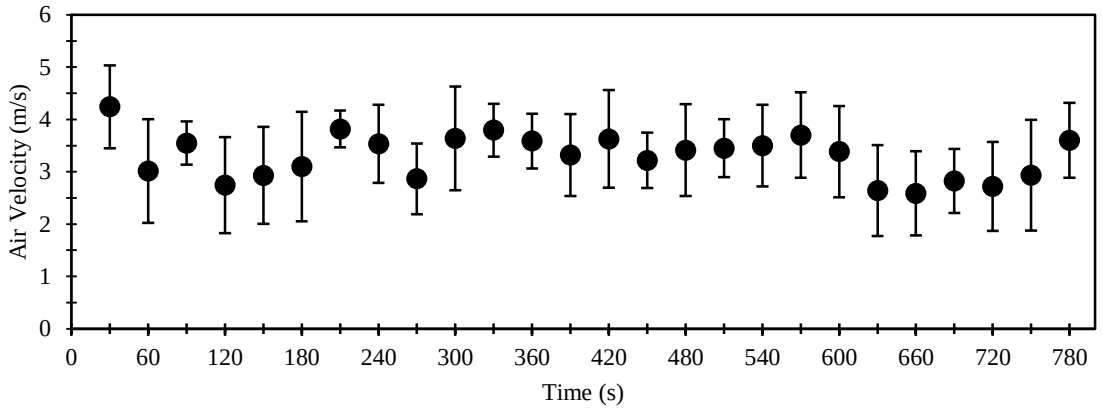

Figure 6:0:1: Wind speed with standard division at Tip (45Hz).

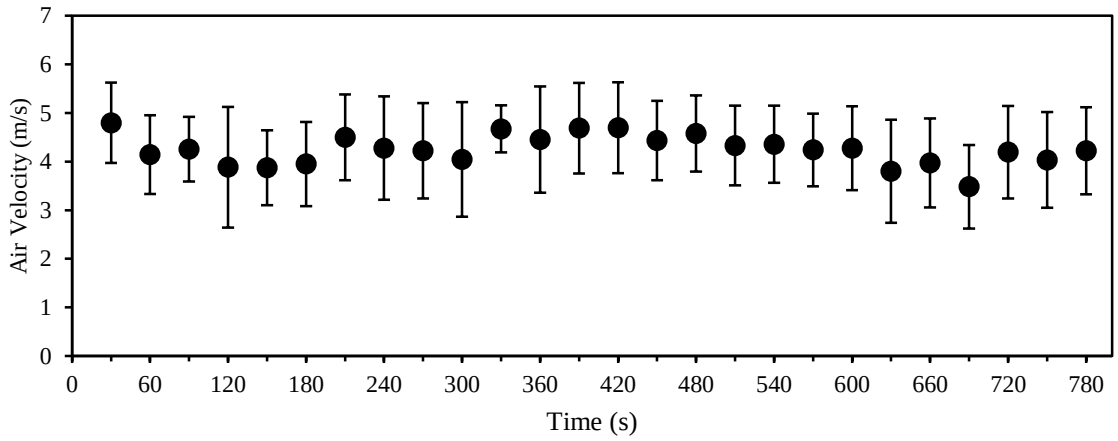

Figure 6:0:2: Wind speed with standard division at Mid 1 (45Hz).

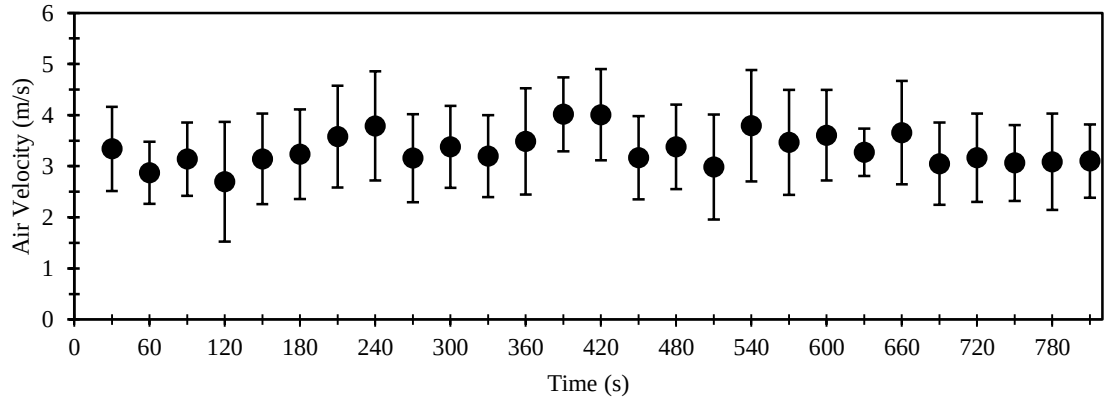

Figure 60:3: Wind speed with standard division at Mid 2 (45Hz).

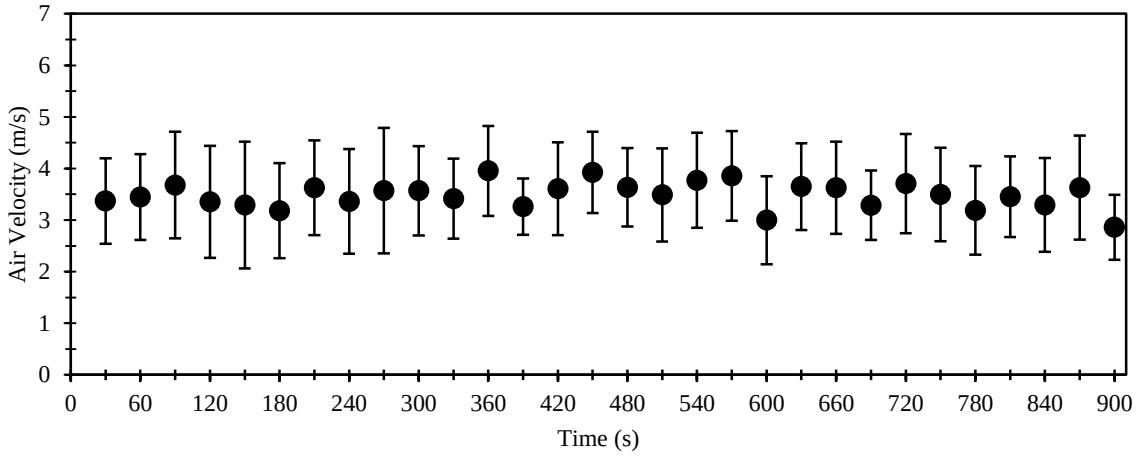

Figure 06:0:4: Wind speed with standard division at Root (50Hz).

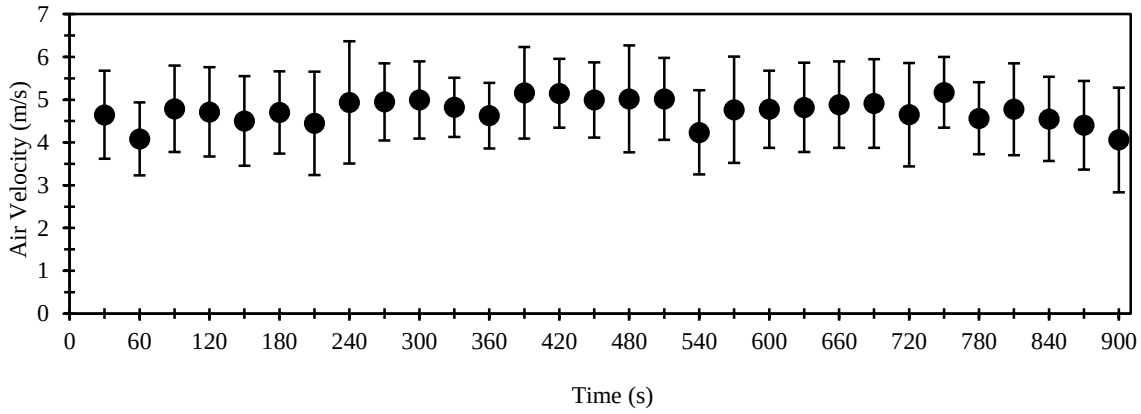

Figure 06:0:5: Wind speed with standard division at Mid 1 (50Hz).

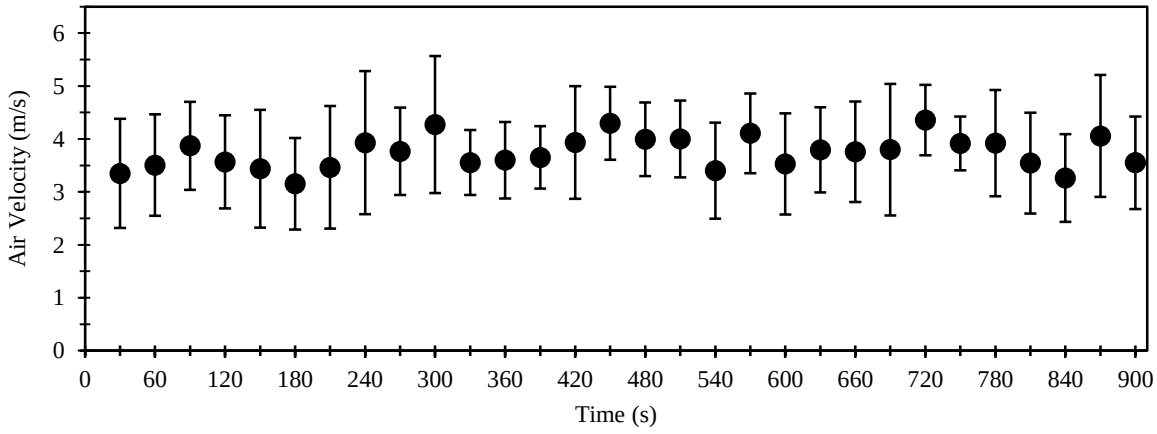

Figure 06:0:6: Wind speed with standard division at Mid 2 (50Hz).

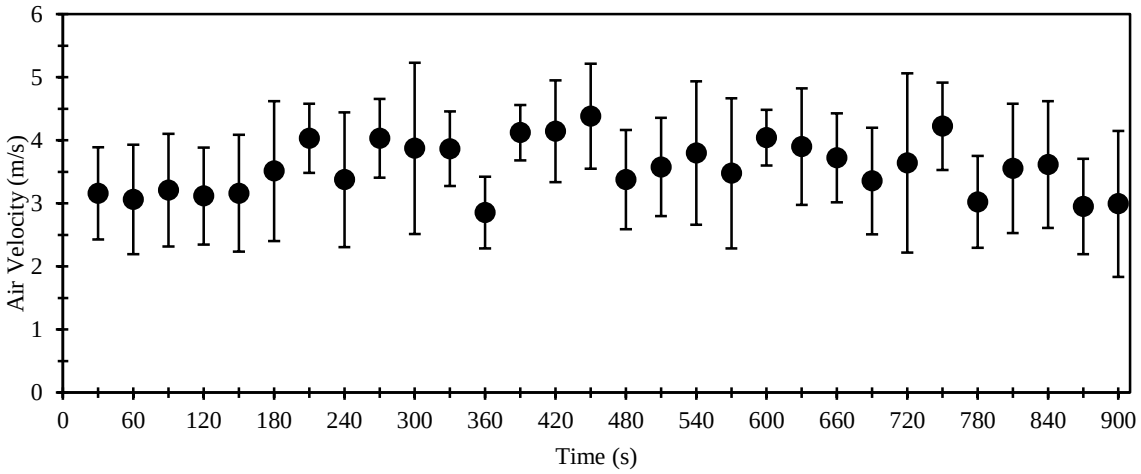

Figure 06:0:7: Wind speed with standard division at Tip (50Hz).

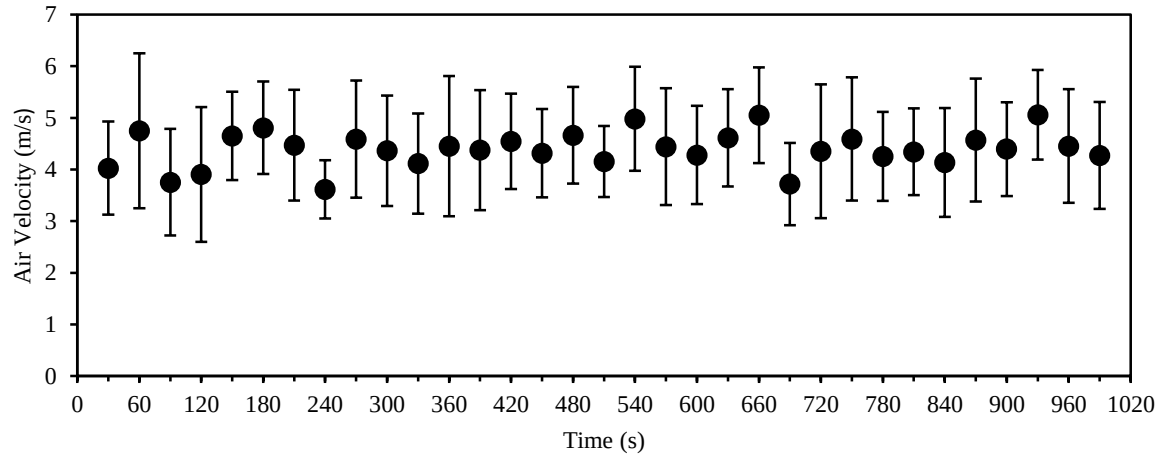

Figure 06:0:8: Wind speed with standard division at Root (60Hz).

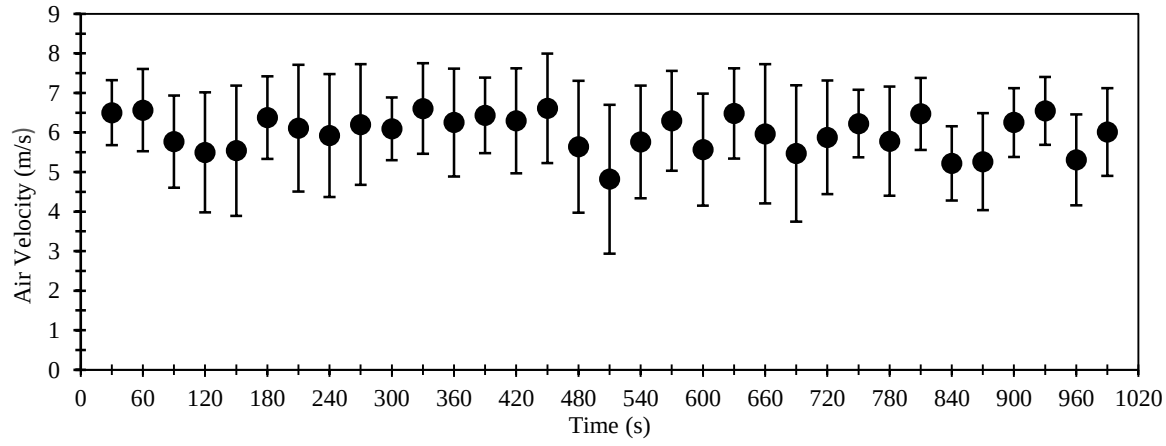

Figure 06:0:9: Wind speed with standard division at Mid 1 (60Hz).

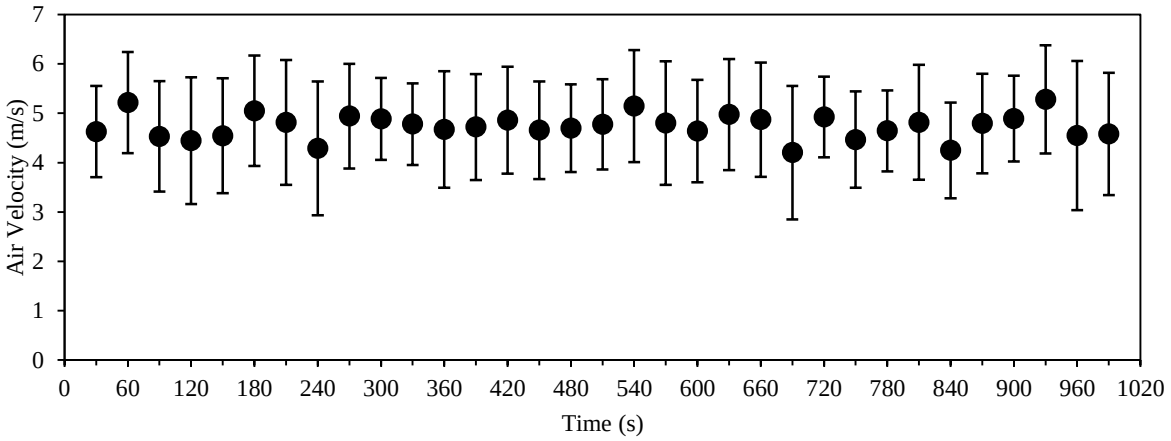

Figure 06:0:10: Wind speed with standard division at Mid 2 (60Hz).

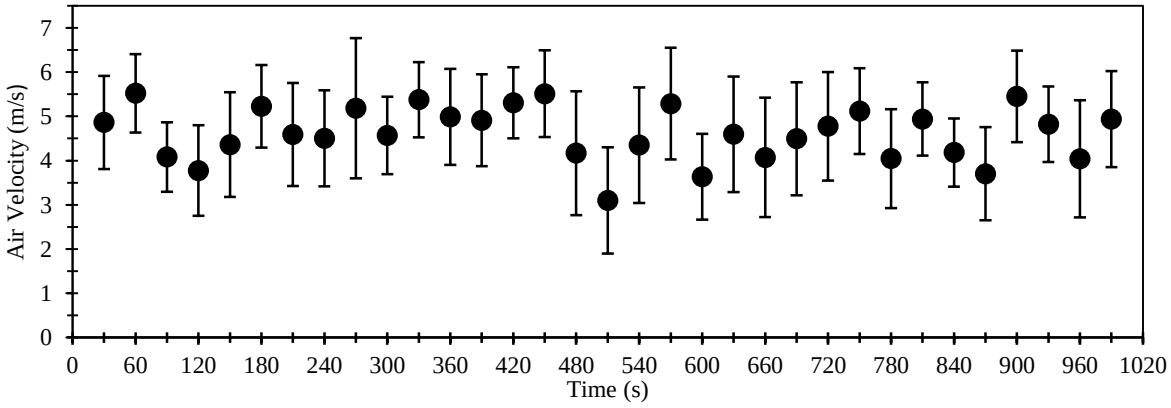

Figure 06:0:11: Wind speed with standard division at Tip (60Hz).

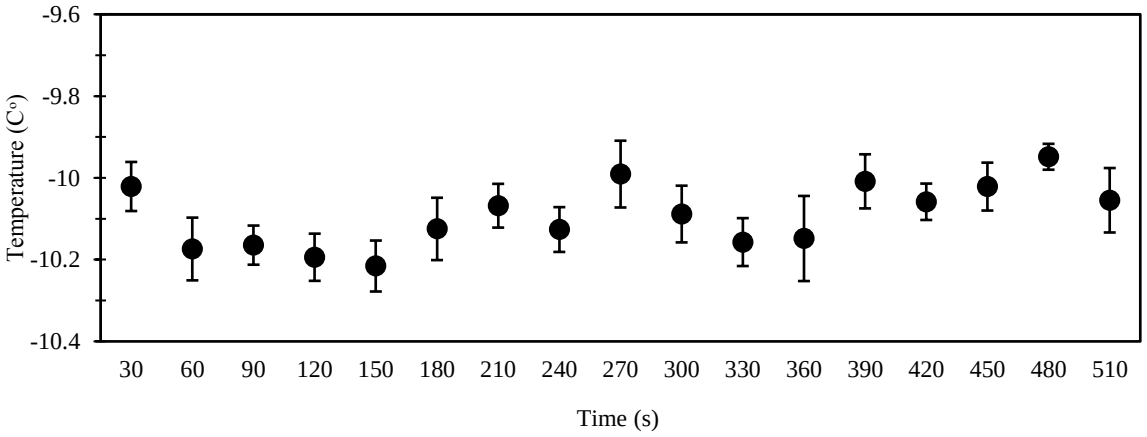

Figure 06:0:12: Temperature during the first hour of the test.

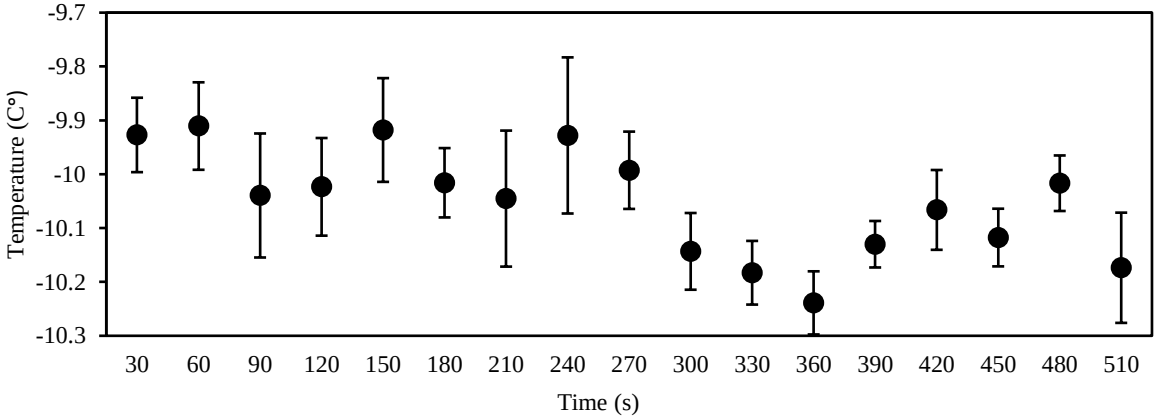

Figure 06:0:13: Temperature during the second hour of the test.

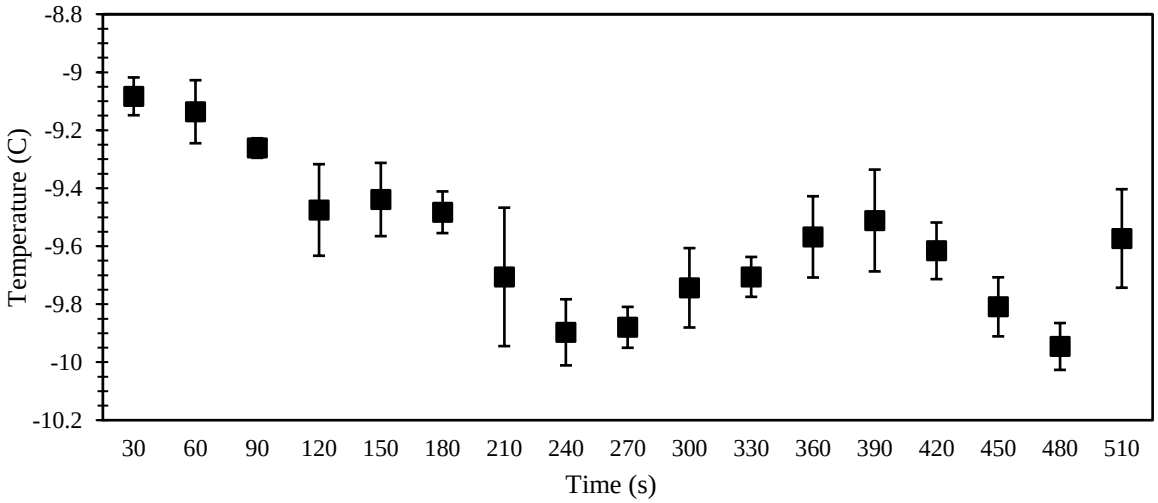

Figure 06:0:14: Temperature during the third hour of the test.